Parkinson's disease-derived α-Synuclein assemblies combined with TNFα and Prostaglandin E_2 induces a specific chronic-type inflammatory phenotype in microglial cells

Cansu Yildirim[1,2,3,4], Alexis Fenyi[5], Pierre Besnault[1,2,3,4], Lina Gomez[1,2,3,4], Julia E. Sepulveda-Diaz[1,2,3,4], Patrick P. Michel[1,2,3,4], Ronald Melki[5], Stéphane Hunot[1,2,3,4]

[1]Sorbonne Université, Paris, France, [2]Institut du Cerveau - Paris Brain Institute - ICM, Paris, France, [3]Inserm UMRS 1127, Paris, France, [4]CNRS UMR 7225, Paris, France, [5]Institut François Jacob, MIRCen, CEA and Laboratory of Neurodegenerative Diseases, CNRS, 92265 Fontenay-aux-Roses, France

Corresponding author: Dr. Stephane Hunot
Institut de Cerveau – ICM, Hôpital de la Salpêtrière, 91 Bd de l'Hôpital, 75013 Paris, France
stephane.hunot@icm-institute.org

Abbreviations:

aSYN	alpha-Synuclein
DIV	day *in vitro*
DLB	dementia with Lewy bodies
DN	dopaminergic neuron
DAM	disease-associated microglia
iMG	induced microglia-like cell
LP	Lewy pathology
LPS	lipopolysaccharide
M1	type-1 macrophage
M2	type-2 macrophage
MSA	multiple system atrophy
PD	Parkinson's disease
PGE_2	prostaglandin E_2
PMCA	protein misfolding cyclic amplification
ROS	reactive oxygen species
TLR	Toll-like receptor
TNFα	Tumor necrosis factor alpha
TPP	TNFα, PGE_2, Pam3CSK4

Abstract

Parkinson's disease (PD) is a common age-related neurodegenerative disorder characterized by the aggregation of α-synuclein (αSYN) building up intraneuronal inclusions termed Lewy pathology. Mounting evidence suggests that neuron-released αSYN aggregates could be central to microglial activation that in turn mounts and orchestrates neuroinflammatory processes potentially harmful for neurons. Therefore, understanding the mechanisms that drive microglial cell activation, polarization and function in PD might have important therapeutic impact. Here, using primary microglia, we investigated the inflammatory potential of pure αSYN fibrils derived from PD cases. We further explored and characterized microglial cell responses to a chronic-type inflammatory stimulation combining PD patient-derived αSYN fibrils (F^{PD}), Tumor necrosis factor-α (TNFα) and Prostaglandin E_2 (PGE_2) (TPF^{PD}). We showed that F^{PD} hold stronger inflammatory potency than pure αSYN fibrils generated *de novo*. When combined with TNFα and PGE_2, F^{PD} polarizes microglial cells toward a particular functional phenotype departing from F^{PD}-treated cells and featuring lower inflammatory cytokine and higher glutamate release. Whereas metabolomic studies showed that TPF^{PD}-exposed microglia were closely related to classically activated M1 pro-inflammatory cells, notably with similar tricarboxylic acid cycle disruption, transcriptomic analysis revealed that TPF^{PD}-activated microglia assume a unique molecular signature highlighting up-regulation of genes involved in glutathione and iron metabolisms. In particular, TPF^{PD}-specific upregulation of *Slc7a11* (coding for the cystine-glutamate antiporter xCT) was consistent with the increased glutamate response and cytotoxic activity of these cells on midbrain dopaminergic neurons *in vitro*. Together, these data further extend the structure-pathological relationship of αSYN fibrillar polymorphs to their innate immune properties and demonstrate that PD-derived αSYN fibrils, TNFα and PGE_2 act in concert to drive microglial cell activation toward a specific and highly neurotoxic chronic-type inflammatory phenotype characterized by robust glutamate release and iron retention.

Introduction

Parkinson's disease (PD) is a common and multi-system neurodegenerative disorder characterized by both motor and non-motor symptoms. The neuropathological hallmark of PD is the progressive and massive degeneration of dopaminergic neurons (DNs) in the *substantia nigra* associated with α-Synuclein (αSYN)-rich deposits building up cytoplasmic inclusions known as Lewy pathology (LP). The aggregation of αSYN may promote several molecular and biochemical defects affecting key cellular functions and driving the progressive demise of DNs (Michel et al., 2016). Beside these toxic cell-autonomous mechanisms, pathological αSYN assemblies can spread from cell to cell to seed aggregates formation in newly contaminated neurons. This prion-like mechanism is believed to contribute to the progression of αSYN pathology across brain networks over time and to be linked to the progressive clinical deterioration of patients (Brundin et al., 2010; Dehay et al., 2015). Accordingly, released extracellular αSYN aggregates may directly interact with and activate surrounding glial cells including microglia to initiate a deleterious inflammatory response. Indeed, evidence from epidemiological, *postmortem*, and animal studies suggest that neuroinflammatory processes associated with glial and immune cell activation participate in the progression of DN cell death (Hirsch & Hunot, 2009).

Microglia, the most abundant tissue macrophages in the brain, executes a number of physiological functions important for the maintenance of tissue homeostasis, synapse remodeling, neurotrophic factor secretion and clearance of debris. Yet, under neurodegenerative conditions and more particularly upon chronic exposure to aberrant proteins, microglial cells mount a persistent sterile (as opposed to infectious) and proinflammatory immune response (Heneka et al., 2015). In PD, a major progress in our understanding of microglial cell activation and related inflammation is the finding that αSYN assemblies behave as true molecular motifs associated with microbes (pathogen-associated molecular patterns or PAMPs). These motifs are recognized by innate immune cells thanks to a panel of immune receptors for recognition of these molecular patterns (pattern recognition

receptors or PRRs) such as Toll-like receptors (TLRs). Thus, mounting evidence suggests that neuron-released αSYN assemblies could be central to microglial cell activation and pathological inflammatory responses through activation of TLRs and other immune-related receptors including CD36 (Lim et al., 2016; Panicker et al., 2019; Scheiblich et al., 2021a; Scheiblich et al., 2021b). Yet, these studies also revealed that the set of receptors involved in this activation crucially depends on the type of αSYN assemblies used in the different experimental setups. Indeed, αSYN can assemble into structurally distinct fibrillar assemblies (also termed polymorphs or strains) that exhibit different phenotypic traits (Bousset et al., 2013; Gribaudo et al., 2019; Shrivastava et al. 2020). As we previously showed, these strains display distinct spreading, tropism, clearance and neurotoxicity in cells and in the rodent brain, which might explain the pathological and phenotypic diversity of different synucleinopathies such as PD, multiple system atrophy and dementia with Lewy bodies (Bousset et al., 2013; Peelaerts et al., 2015; Gribaudo et al., 2019; Rey et al., 2019; Shrivastava et al. 2020). Importantly, we recently strengthened this concept using patient-derived αSYN strains generated by protein misfolding cyclic amplification (PMCA) (Van der Perren et al., 2020). Besides demonstrating a structure-pathology relationship we brought evidences for differences between patient-derived and *de novo* generated αSYN strains (Van der Perren et al., 2020). Together, these data suggest that the intrinsic structure of fibrillar αSYN is a major determinant of their biological properties. A likely explanation for this structure-function relationship is the fact that differences in surface accessibility contribute to the differential binding of distinct αSYN strains to partner proteins such as cell surface receptors (Shrivastava et al. 2020; Landureau et al., 2021). Hence, whether patient-derived αSYN strains display similar or different inflammatory properties to previously described *novo* generated αSYN strains is unknown but their use in model systems have the potential to better model disease-associated microglial activation and perhaps contribute to more relevant knowledge.

An often neglected, but important issue for understanding the pathomechanisms linked to innate inflammation in PD is to comprehensively define the complex network of stimuli that drive microglial cell activation and function. Most cell culture models to study microglia-associated immunity

in PD have been developed upon exposure of microglial cells to the prototypical bacterial inflammogen lipopolysaccharide (LPS) or, much elegantly, to different types of recombinant αSYN aggregates of various purity as a disease-specific trigger and TLR activating pathological ligand (Song et al., 2020; Tu et al., 2019; Scheiblich et al., 2021a; Scheiblich et al., 2021b). Although these models have brought invaluable knowledge about molecular mechanisms and pathways of microglial cell activation, they remain limiting in that they do not consider specific aspects of PD neuroinflammation which is chronic in nature, and which most likely involves a combinatory action of several mediators present in the inflammatory milieu. It is now well established that the phenotypes and functions that activated microglia can adopt are diverse and strongly depend on the nature, intensity and complexity of stimulation to various cues (Perry et al., 2010). Far from the original idea that macrophages can be polarized into classically (M1) or alternatively (M2) activated cells representing two polar extremes of molecular programming, there are now compelling evidences suggesting that they can adopt a much larger spectrum of activation states associated with different phenotypes and, presumably, functions (Chiu et al., 2013; Xue et al., 2014). Of particular interest, it has been shown that human macrophages engage a specific molecular program and adopt a unique phenotype when exposed to a chronic-type inflammatory stimulus made up of Tumor necrosis factor (TNF)-α, Prostaglandin E_2 (PGE_2) and TLR2 ligand such as the synthetic molecule Pam3CSK4 (referred as "TPP" stimulation) (Xue et al., 2014). These inflammatory factors are commonly found in chronic inflammatory conditions such as Mycobacterium tuberculosis-associated granulomatous diseases, or granulomatous listeriosis (Ciofani et al., 2012; Marino et al., 1997; Popov et al., 2006; Reiling et al., 2002; Shay & Celeste Simon, 2012). Remarkably, they are elevated in the brain of PD patients as well, αSYN aggregates being the most likely pathological ligand of TLR2 whose expression is tightly linked to PD pathogenesis (Doorn et al., 2014; Hunot et al., 1996; Wu et al., 2007), suggesting that they may act in concert to shape microglial activation into a unique disease phenotype. Yet, cell-specific immune properties might be important and whether microglial cells behave similarly to peripheral macrophages upon chronic-type inflammatory stimulation has not been explored.

In this study, using a model system of cultured primary microglial cells, we sought to document the inflammatory properties of patient-derived αSYN strains and to determine whether microglia exposed to PD-relevant inflammatory cues in a novel and original combinatory approach adopt a specific molecular phenotype and function. We found that PD patients-derived αSYN fibrils hold stronger inflammatory properties than αSYN fibrils assembled *de novo*. We also show that compared to classical M1-shaped microglia (LPS-induced), cells simultaneously exposed to PD patients-derived fibrils, TNFα and PGE_2 assume a unique chronic-type inflammatory molecular signature associated with higher glutamate release and iron retention propensities.

Materials and Methods

Animals

Animal care and housing were conducted in accordance with recommendations of the European Union Council Directives (2010/63/EU). Experimental procedures were authorized by the Committee on the Ethics of Animal Experiments Charles Darwin N°5 under the registration number Ce5/2017/005. C57BL/6J mice were obtained from Janvier LABS (Le Genest St Isle, France).

Reagents and antibodies

Leibovitz's L-15 medium (Thermo Fisher Scientific, Illkirch, France, #11415049), Dulbecco's Modified Eagle Medium/F-12 nutrient mixture (DMEM; Thermo Fisher Scientific, #31885023), Neurobasal-A medium (Nba; Thermo Fisher Scientific, #10888022), B27 supplement minus antioxidants (Thermo Fisher Scientific, #10889038), N2 mix (Thermo Fisher Scientific, #17502048), RPMI-1640 Glutamax (Invitrogen, #61870010), RPMI-1640 (Thermo Fisher Scientific, #21875034), penicillin/streptomycin (Thermo Fisher Scientific, #15140122), antibiotic/antimycotic solution (Invitrogen, #15240062), Trypsin 0.05% EDTA (Thermo Fisher Scientific, #25300054), polyethylenimine (PEI; Sigma-Aldrich, #P3143), Histopaque-1077 (Sigma, #10771-500M), fetal bovine serum (FBS; Biowest, #S1820-500), Nitrotetrazolium Blue chloride (Sigma-Aldrich, #N6876), Pam3CSK4 (Invivogen, tlrl-pms), Lipopolysaccharides (LPS) from Escherichia coli O26:B6 (Sigma-Aldrich, #L8274), recombinant human TNFα (Sigma-Aldrich, #H8916), PGE_2 (Sigma-Aldrich, #P6532), recombinant mouse IFNγ (Immunotools, #12343537), recombinant mouse IL4 (Immunotools, #12340045), recombinant human GM-CSF (R&D, #215-GM-010), recombinant human IL34 (R&D, #5265-IL-010), Sulfasalazine (Sigma, S0883), MK-801 (Tocris, #0924), Cytotoxicity Detection Kit (LDH; Roche, #11644793001), Amplex Red Glutamic Acid/Glutamate Oxidase Kit (Thermo Fisher Scientific, #A12221), NucleoSpin RNA XS, RNA purification kit (Macherey-Nagel, #740902.50), SYBR Green reactifs (LightCycler® 480 SYBR Green I Master; Roche, #04707516001), StraightFrom® LRSC CD14 MicroBead Kit (Miltenyi, #130-117-026), MACS BSA Stock Solution (Miltenyi, #130-091-376), autoMACS® Rinsing Solution (Miltenyi, #130-091-222). Anti-mouse

CD25 (BioRad, MCA1260), anti-mouse CD11b (BioRad, MCA74G), anti-human CCR2 (R&D Systems; MAB150-100), anti-human CX3CR1 (BioRad, AHP566). Mouse TNFα ELISA Kit (Thermo Fisher Scientific, BMS607-3), Mouse IL6 ELISA Kit (Thermo Fisher Scientific, BMS603-2TWO), Mouse IL1β ELISA Kit (Thermo Fisher Scientific, BMS6002), Mouse IL10 ELISA Kit (R&D Systems, M1000B), U-Plex (Meso Scale Discovery, K15069L-1), Mouse Pro-Inflammatory 7-Plex Tissue (Meso Scale Discovery, K15012B-1), Mouse IL1α ELISA Kit (Biolegend, #433404), Mouse CXCL5 ELISA Kit (R&D Systems, MX000), Hoechst 33342 (Tocris, #5117).

Human brain tissue collection and preparation of αSYN assemblies

Brain tissues from patients suffering from PD (n=4) and DLB (n=4) were obtained at autopsy from the UK Brain Bank (Imperial College London, UK). The clinicopathological description of the patients is detailed elsewhere (Van der Perren et al., 2020). After histological identification of LP-rich regions, the cingulate cortex was isolated from the brains and processed into brain homogenates. Patients-derived αSYN assemblies were obtained by protein misfolding cyclic amplification (PMCA) as described elsewhere (Van der Perren et al., 2020). Briefly, frozen brain tissues were diluted 1:5 (w/v) in PMCA buffer (150 mM KCl, 50 mM Tris–HCl pH 7.5) and sonicated for 1 min, with 10 s pulses followed by 10 s pauses (SFX 150 Cell Disruptor sonicator equipped with a 3.17 mm Branson microtip probe). Brain homogenates were further diluted in PMCA buffer containing monomeric αSYN (100 µM) to a final concentration of 2% (w:v). PMCA amplification (4 cycles) was performed using the Q700 generator and a 431MPX horn (Qsonica, Newtown, CT, USA) with the following sequence: 15 s of sonication and 5 min pause at 31 °C. Cycle 2, 3 and 4 were performed using 1% of the preceding cycle reaction as seeds. At cycle 4, PMCA reactions products were spun for 30 min at 50,000g and the pelleted assemblies were resuspended in phosphate-buffered saline (PBS) buffer at a 100µM final concentration. Prior usage, assemblies were fragmented by sonication for 20 min in 2-ml Eppendorf tubes in a Vial Tweeter powered by an ultrasonic processor UIS250v (250 W, 2.4 kHz; Hielscher Ultrasonic, Teltow, Germany), aliquoted, flash frozen in liquid nitrogen and stored at -80 °C. Recombinant αSYN fibrils were prepared

and characterized as previously described (Bousset et al., 2013). In preliminary studies, we observed similar inflammatory activities of patient-derived αSYN fibrils in cultured microglial cells between each patient of a given disease group (data not shown). Therefore, we prepared a single batch of PD and DLB patients-derived αSYN fibrils by mixing at equal amount the assemblies generated from the 4 patients of each disease group.

Transmission electron microscopy

The morphology of PMCA-amplified αSYN assemblies (3rd cycle) was assessed by transmission electron microscopy (TEM) using a Jeol 1400 transmission electron microscope following adsorption onto carbon-coated 200 mesh grids and negative staining with 1% uranyl acetate. The images were acquired using a Gatan Orius CCD camera (Gatan, Elancourt, France).

Primary mouse microglia culture

Primary mouse microglia were isolated and cultured following a protocol previously described (Sepulveda-Diaz et al., 2016). Newborn pups were sacrificed and the whole brain rapidly dissected out. After mechanical dissociation of the brain tissue, cells in suspension were plated onto polyethyleneimine-coated T-75 flasks with 12 ml of DMEM supplemented with 10% FBS and antibiotics (2 brains per flask). At DIV2, medium was completely changed to the fresh medium and then cultures were let grown without medium change until completion of microglial cell isolation (DIV14–18). For microglial-conditioned medium (MCM) transfer onto neuronal culture experiments, microglial cells were grown and stimulated in DMEM-based astrocyte-conditioned medium (ACM) prepared as described below.

Microglia cell seeding and stimulation

Cultured microglia were washed 3 times with DMEM and incubated for 5 min with 5 mL pre-warmed (+37°C) trypsin. DMEM containing 10% FBS (10 mL) was then added to abrogate trypsin activity and cells were collected in an ice-cold 50 mL falcon tube before centrifugation at 188 x g for 6 min at 4°C.

The cell pellet was then resuspended in DMEM-1% FBS. Cells were plated at a density of 90,000 to 110,000 cells/cm^2 and incubated for 24h at 37°C for complete settlement. Microglia were stimulated for 24 to 48 hours with LPS (10 ng/mL), Pam3CSK4 (1 µg/mL), TNFα (800 IU/mL), PGE_2 (1 µg/mL) or fibrillar αSYN assemblies at various concentrations. When indicated, stimulation factors were used in combination.

Astrocyte-conditioned medium

Astrocyte-conditioned medium (ACM) was prepared from primary cultures of astrocytes obtained from C57BL/6J mouse neonate (P0) brains as described elsewhere (Tourville et al., 2022). Briefly, brains were dissected and dissociated by mechanical trituration in L15 medium. After centrifugation, cell pellet was resuspended into DMEM/F-12 plus 10% FBS and dissociated cells were distributed and let grown on laminin-coated T-75 flasks. At DIV2, medium was replaced by fresh DMEM/F-12 plus 10% FBS and clodronate-loaded liposomes (2.6 µg/mL; Liposoma BV, Netherlands) were added twice weekly to discard residual macrophages. Twelve to fourteen days later (DIV14-16), culture medium was totally removed and replaced by either DMEM or Neurobasal-A (Nba) supplemented with 2% B27, 1% N2 and 1% antibiotics. After three additional days of culture, the DMEM-based and Nba-based ACM were recovered, filtered (0.2µm pores) and frozen at −20 °C until use.

Primary mouse midbrain culture

Primary mouse midbrain cultures were prepared as described before (Tourville et al., 2022). Briefly, embryos (E13.5) from pregnant C57Bl6 females (Janvier LABS, Le Genest St Isle, France) were collected in L15 medium and midbrain was dissected out under a binocular microscope. Midbrain tissue was digested in Trypsin plus 0.05% EDTA (Thermo Fisher Scientific, #25300054) for 20 min at +37°C and Trypsin-dissociated tissue was then mechanically triturated by gentle pipetting (8–10 strokes) using a Gilson pipette fitted with a sterile polypropylene blue tip with no filter (StarLab France, Orsay, France). After 10 min of sedimentation on ice, the supernatant was collected, and trituration and sedimentation steps were repeated one more time. Collected supernatant was then centrifuged at 317xg for 5 min at

+4°C. Cell pellet was resuspended in L15 medium and dissociated cells were distributed in PEI-coated Nunc 48 well-plates (Roskilde, Denmark) in Nba medium supplemented with 2% B27, 1% N2, 1% antibiotics at a density of 0.4 midbrains/well. After 1-2 hours incubation, ARA-C (1.2µM; Sigma-Aldrich, C1768) was added to curtail astrocyte proliferation. At DIV 1, ARA-C was brough to a 1.6 µM final concentration and at DIV 2, culture medium was fully replaced by Nba-based ACM. Serum-free ACM-based protocols were shown to improve neuronal maturation, electrical activity and long-term viability compared to classical Nba/B27 or FBS-based cell culture media (Pozzi et al., 20017).

Quantification of ROS level

To determine intracellular production of superoxide anions upon stimulation we used nitro-blue tetrazolium chloride (NBT) reagent following a protocol adapted from Rook et al. (1985). In brief, 100 000 cells were seeded in 48-well plate and stimulated as mentioned above for 24h. One hour and half before the assay, NBT (500 µM) was added in each well and cells were further incubated before washing twice with warm PBS at 24hr after stimulation. Then, 100 µL of absolute methanol was added in each well and culture plates were left under the fume hood until methanol evaporation. After complete drying, 60 µL of 2M KOH and 70 µL of DMSO were added in the wells and incubated under mild agitation for 5-10 minutes after what absorbance at 620 nm was measured. Results were normalized to NSC experimental condition.

Cytokine and glutamate assays

Cytokine levels were measured using ELISA kits or MSD U-Plex plates (Meso Scale Diagnostics) according to the manufacturer’s instructions. Absorbance measurements were performed at 450 nm. Glutamate levels were measured using the Amplex Red Glutamic Acid/Glutamate Oxidase Kit according to the manufacturer's instructions. The quantification was carried out on 10 µl of culture medium samples. The fluorescent reaction product resulting from glutamic acid oxidation was quantified using excitation and emission wavelengths of 545 and 590 nm, respectively. Absorbance

and fluorescence measurements were performed using the SpectraMax i3X microplate reader (Molecular Devices, Sunnyvale, CA).

Transcriptomic analysis

To determine transcriptomic changes evoked by the different inflammatory stimulations, $1x10^5$ microglial cells were seeded in 48-well plates and then stimulated or not (NSC) with LPS (10 ng/ml) or TPF^{PD} for 24h. Seven to eight biological replicates per condition from two independent experiments were used. RNA was isolated using NucleoSpin® RNA XS kit and their quality evaluated with an Agilent 2100 Bioanalyzer (Agilent Technologies). All RNA samples had RNA integrity numbers (RINs) greater than 7. We produced libraries for 3'-mRNA sequencing using 200 ng purified RNA per sample processed with TruSeq Stranded RNA kit (Illumina, San Diego, CA) according to the manufacturers' protocol. Paired-end sequencing was then performed on the Illumina NextSeq 500 and NovaSeq 6000 platforms with a sequencing depth of 80 million reads per sample (iGenSeq core facility, ICM, Paris France). All samples were assessed separately for overall read quality using FASTQC. Reads were trimmed using the Trimmomatic tool (Illumina), and then aligned to the mouse genome using Top-Hat (Illumina) and fragments were assigned to genes using FeatureCounts program (iCONICS core facility, ICM, Paris France). Differentially expressed genes (DEGs) were analyzed using the open source Bioconductor package DESeq2 in R software (Love et al., 2014) (Log2FC > 0.5; FDR-adjusted p value < 0.05). Pathway enrichment analysis was performed using the open source gene enrichment analysis tool Enrichr (Chen et al., 2013; Kuleshov et al., 2016; Xie et al., 2021). Data visualization and biological interpretation were performed with GraphPad Prism 7.0 software.

Metabolomic analysis

Metabolite profiling analysis was carried out on an Acquity UPLC system (Waters Corp, Saint-Quentin-en-Yvelines, France) coupled to a hydrid Orbitrap- and Q-Exactive-based instrument (Thermo Fisher Scientific, Illkirch, France). To analyze and compare microglial cell metabolome under different inflammatory conditions, we performed an untargeted metabolomic analysis of cells stimulated or not

with LPS (10 ng/mL) or TPF^{PD} for 48 hours. Five biological replicates for each condition were prepared. Approximately $1x10^6$ cells grown in $25cm^3$ flasks were lysed using a methanol-based method consisting in adding 1 mL of frozen methanol (-20°C) followed by 5 min incubation on dry ice and 5 min rest at room temperature. This incubation cycle was repeated 3 times before collecting cells with the help of a cell scraper and transferred to a 50mL falcon tube. Samples were kept frozen at -80°C until use. Sample preparation for LC-MS analysis was as followed: Prior to extraction, cells were homogenized in 100µL of H_20 including 0.1% formic acid and internal standards (mix of 16 labelled amino acids at 10 µg/mL) to a final concentration of 2500 cells/µl. Six cycles of freeze-thaw were applied for cell lysis. Then, 4 volumes of frozen methanol (−20 °C) containing equimolar (10 µg/mL) mix of internal standard [16 labelled amino acids and 3 labelled nucleotides (ATP,$^{15}N_5$; ADP,$^{15}N_5$ and AMP,^{13}C,$^{15}N_5$)] were added to 100 µL of sample and then vortexed. Samples were further sonicated for 10 min before being centrifuged at 10,000×g and +4°C for 2 min and let for one hour (+4°C) for slow protein precipitation. Samples were then centrifuged at 20,000×g (+4 °C) for 20 min and supernatants were transferred to new tubes and dried out before being reconstituted in a solution of water/acetonitrile (40:60; v-v). Chromatographic conditions and experimental settings were as described before (Garali et al., 2018). Briefly, LC-MS analysis was performed with a ZIC-*p*HILIC chromatographic column (5 µm, 2.1 × 150 mm, Merck, Darmstadt, Germany). Full scan positive and negative ionization mode with a resolution of 70.000 (FWHM) and a scan range of m/z 50–750 were used. The mass spectrometer was systematically calibrated in both ion polarity modes with the Pierce calibration solution. Injection volume was set to 10 µL. The mobile phase (flow rate of 0.2 mL/min for 29 min) consisted in 10 mM of ammonium carbonate at pH=10.5 (A) and acetonitrile (B). MS data processing was performed using XCMS R package with CentWave algorithm and CAMERA tools implemented in R software and the galaxy workflow4metabolomics (Giacomoni et al., 2015; Smith et al., 2006; Tautenhahn et al., 2012). Processing steps included peak picking, peak grouping, retention time correction and annotation of isotopes and adducts. Processed LC-MS data were further analyzed based on standard protocols (Dunn et al., 2011; Want et al., 2010) and resulted in a data matrix in which each metabolomic feature was

characterized by a retention time (RT), a mass to charge ratio (m/z), its corresponding intensities and the isotope-adduct annotation from CAMERA tool. Metabolomics data matrix was then filtered, normalized, curated and log-10 transformed based on quality assurance (QA) strategy (Dunn et al., 2012; Veselkov et al., 2011). Of note, peaks with more than 30% of missing values were discarded. Data visualization for biological interpretation was performed with Multi Experiment Viewer (MeV) statistical software package (version 4.9.0; http://www.tm4.org/mev/) (Saeed et al., 2003). This software was used to perform principal components analysis (PCA), heatmaps and tests to compute a p-value for each metabolic feature with a threshold of significance set to 0.05. False discovery rates (FDR) were corrected using the Benjamini-Hochberg method (Benjamini & Hochberg, 1995) to adjust p-values for false discovery involving multiple comparisons.

Quantitative real-time PCR

Total RNA was isolated using an extraction kit according to the manufacturer's instructions (Macherey-Nagel). RNA concentration was assayed with a NanoDrop (Thermo Scientific) and adjusted with nuclease-free water at equal concentration for all samples. RNA was then reverse transcribed to cDNA using the Verso cDNA Synthesis Kit (Thermo Scientific) following manufacturer's instructions. In brief, RNA was denatured at 70°C for 2 min. Then kit mix was added to each tube. Samples were the subjected to successive incubation: 25°C for 10 min, 42°C for 1h and 85°C for 5 min.

Quantitative PCR assay was designed to include three technical replicates per sample and two reference genes (*Rab7* and *Sdha* for primary mouse microglia; *Ubc* and *Sdha* for human microglia-like cells) that were selected upon analysis of gene expression stability across the different experimental conditions (geNorm tool of qBasePlus software, Biogazelle) and among 8-10 initial gene candidates. Quantitative PCRs were performed using a LightCycler® 480 System using compatible SYBR Green reagents (LightCycler® 480 SYBR Green I Master). PCR program was: 95°C for 10 min, 45 cycles of 95°C for 15 sec and 60°C for 60 sec, then cooling. All generated data were further processed and analysed with qBasePlus.

Generation of human induced microglia-like cells

According to good clinical practice, the protocol used for collecting human peripheral blood mononuclear cells has been approved by an ethical committee affiliated to French regulation authorities (CCPPRB Groupe Hospitalier Pitié-Salpêtrière, Paris, France). Samples were collected from a healthy donor (49-year-old male) who signed informed consent and who was included in an INSERM-sponsored clinical study. Human induced microglia-like cells (iMGs) were obtained following the protocol published by (Ohgidani et al., 2015) with some modifications. Briefly, 10 mL blood samples were collected in EDTA, and peripheral blood mononuclear cells (PBMCs) purified by density gradient (Histopaque-1077) centrifugation at 400xg for 30 min. After isolation, they were washed in RPMI-1640 medium and centrifuged at 300xg for 10 min. Cell pellet was resuspended in separation buffer (MACS BSA stock solution/AutoMACS® Rinsing Solution at 1/20 dilution) and passed through MACS SmartStrainers (30 µm) to eliminate cell clumps. Monocytes were then isolated using 250µL of StraightFrom LRSC CD14 MicroBeads added to 40 mL of cell suspension. Cells and beads were incubated 15 min at +4°C and centrifuged at 300xg for 10 min. Cell pellet was resuspended in the separation buffer and labelled cells were separated by LS columns on the QuadroMACS™ Separator and recovered in Whole Blood Column Elution Buffer. After centrifugation at 300xg for 10 min, cell pellet was resuspended in RPMI-1640 Glutamax supplemented with 10% FBS and 1% antibiotic-antimycotic solution. Monocytes were then seeded at a concentration of $6x10^4$ cells/well in 96 well-plates and incubated overnight at 37°C with 5% of CO_2. To induce differentiation, the medium was changed at DIV1 with RPMI-1640 Glutamax containing recombinant human GM-CSF (10 ng/ml) and recombinant human IL34 (100 ng/ml). Differentiating medium was freshly renewed at DIV6. On day 27 following cell seeding, differentiated iMGs were used for inflammatory stimulation assay.

Cell immunostaining and quantification

Primary microglial cells and iMGs were fixed with 3.7% formaldehyde solution (Sigma-Aldrich, 252549) for 12 min and then washed twice with PBS. Primary mouse microglia were then incubated overnight

at +4°C with rat anti-CD25 (1/100) or rat anti-CD11b (1/100) antibodies diluted in PBS. Then, they were washed three times with PBS followed by incubation with anti-rat IgG coupled with Alexa488 fluorophore (1/300 dilution) for 2 hours at RT. For double immunofluorescent staining of iMGs, cells were incubated overnight at +4°C with rabbit anti-CX3CR1 and mouse anti-CCR2 primary antibodies (diluted at 1/500 in PBS containing 0.1% Triton-X 100 and 5% NGS). Cells were then rinsed three times with PBS and then incubated with anti-rabbit IgG coupled with Alexa488 fluorophore and anti-mouse IgG coupled with Alexa546 fluorophore (1/300 dilution) for 1 hour at RT. Following two washing steps with PBS, immunostained cells were further stained with Hoechst (1/4000 dilution) for 10 min and rinsed three more times with PBS. The ratio of CX3CR1 to CCR2 was calculated by fluorescent signal intensity quantified using an automated quantitative imaging platform (ArrayScan, ThermoFisher). Representative images were acquired using an Axio Observer 7/Apotome microscope (Zeiss). For midbrain cultures, similar immunodetection protocol was used to assess tyrosine hydroxylase (TH), a dopaminergic neuronal marker. Cells were incubated at +4°C for 24hr in mouse anti-TH primary antibodies (LNC1, Immunostar, #22941) diluted at 1/2500 in PBS plus 0.2% Triton-X 100, then rinsed three times and incubated for 2 hours at room temperature in Alexa Fluor 488-conjugated goat anti-mouse secondary antibodies (1/300 dilution, Thermo Fischer Scientific). Following two washes in PBS, cells were stained with Hoechst 33342 (1/4000 dilution; Tocris, 5117) for 10 min. Neuron culture images were acquired with a Nikon Eclipse Ti-U fluorescence inverted microscope (Nikon France, Champigny sur Marne, France) equipped with a Hamamatsu's ORCA-D2 camera and HCImage software (Hamamatsu Photonics, Massy, France). The number of TH+ neuron/culture well was estimated by visually inspecting samples with a 10× objective over 10–15 visual fields that were randomly selected for each treatment condition.

Statistical analysis

Statistics were analyzed using SigmaPlot 14.0 or GraphPad Prism 7.0 software. Results are expressed as means ± standard error of the mean (SEM). Normality of data distribution was assessed with the

Shapiro-Wilk test. Statistical significance of normally distributed data was assessed using Student's t-test for comparison between two groups and ANOVA followed by Tukey's post-hoc test for multiple comparisons. When data were not normally distributed, significance was determined with Mann-Whitney U test for comparison of two groups and Kruskal-Wallis test followed by Dunn test for multiple comparisons. Statistical significance level was set as follows: * p value < 0.05, ** p value < 0.01, *** p value < 0.001.

Results

Generation and characterization of patient-derived αSYN assemblies

To investigate the inflammatory properties of patient-derived αSYN aggregates we first generated pure *in vitro* amplified αSYN fibrillar assemblies using a protein misfolding cyclic amplification assay (PMCA) applied on LP-rich PD and DLB brain tissue homogenates as described elsewhere (Van der Perren et al., 2020). A detailed structural and biochemical characterization of this PMCA-amplified pathological material demonstrates that fibrillary assemblies derived from PD patients (F^{PD}) are structurally different from those obtained from DLB patients (F^{DLB}). Thus, TEM analysis revealed disease-specific differences in the shape of the fibrils with PD patient-derived αSYN fibrils exhibiting a relatively flat and twisted appearance whereas those derived from DLB patients were cylindrical and not twisted (Figure S1). Furthermore, assemblies from individual PD or DLB patients have comparable limited proteolysis pattern and morphology suggesting the existence of disease-specific αSYN strains (Van der Perren et al., 2020).

PD-derived αSYN assemblies evoke robust inflammatory response in primary microglial cells

We evaluated and compared the inflammatory potential of PD patients-derived αSYN fibrils by exposing primary microglial cells to equal concentration (3µM) of either F^{PD} or well-characterized αSYN fibrils generated *de novo* (F^{S}) (Bousset et al., 2013; Scheiblich et al., 2021). As a positive control of inflammatory microglia, cells were treated with LPS (10ng/ml), a prototypical inflammogen and ligand for TLR4 (Döring et al., 2017). After 48 hours of treatment, stimulated microglia undergo morphological changes as compared to non-stimulated control cells (NSC) (Figure 1A). In particular, LPS-exposed cells lost their ramified and spindle-shaped processes adopting more flattened and wider morphology typical of inflammatory induction (Sepulveda-Diaz et al., 2016). Of note, F^{S} and F^{PD} treatment induces similar morphological changes as those observed with LPS stimulation suggesting inflammatory activation by αSYN fibrillar assemblies. To get further insights into the inflammatory potential of F^{PD},

we evaluated the production and release of several inflammatory cytokines in response to increasing amount of F^{PD} ranging from 0.01 to 3µM. We observed a dose-dependent increase in both TNFα, IL6 and IL10 release after 24 hours of treatment (Figure 1B) with an efficient and significant cytokine release at F^{PD} concentrations of 1µM and above (Figure 1B). As inflammatory microglial cells, in particular when exposed to fibrillary aggregates of αSYN, can release large amount of glutamate (dos-Santos-Pereira et al., 2018), we measured glutamate concentrations in microglial cell culture medium after exposure to F^{PD}. As shown in Figure 1B, F^{PD} evokes strong glutamate release from microglial cells in a dose-dependent manner within F^{PD} concentration range 1.5 and 3µM (3- and 11-time increase compared to NSC, respectively). Whereas both F^{PD} and F^{S} efficiently trigger inflammatory-associated morphological changes in microglial cells (Figure 1A), we found that F^{PD} were more potent than F^{S} in inducing cytokine and glutamate release after 48 hours of stimulation. Indeed, at equal αSYN assembly concentration (3µM), F^{PD} induces 5-, 17- and 3-times more TNFα, IL6 and IL10 than F^{S}, respectively (Figure 1C). Similarly, extracellular amount of glutamate following exposure to F^{PD} was twice as much as in F^{S}-stimulated cells (Figure 1C). Interestingly, we observed that microglia-associated inflammatory responsiveness toward F^{DLB} was even more important than that evoked by F^{PD} assemblies (Figure 1C). Together, our data not only show that F^{PD} hold potent inflammatory properties on microglial cells, but also, that PD-derived assemblies display stronger and lower stimulatory properties than αSYN fibrils generated *de novo* and F^{DLB}, respectively. Given the structural differences on one hand between F^{PD} and F^{S} , and on the other hand, between F^{PD} and F^{DLB} (Bousset et al., 2013; Van der Perren et al., 2020), our data also suggest structure-function relationship regarding the inflammatory properties of αSYN aggregates on brain tissue macrophages and argue for the use of PD-derived material to better model disease-associated inflammatory mechanisms.

Chronic-type stimulation of microglia is associated with lower cytokine but higher glutamate release.

Chronic inflammatory conditions in human are associated with sustained high tissue levels of TNFα, PGE_2 and innate immune receptor activating ligands acting in concert to shape macrophage response. Combinatory stimulation of human macrophages with these factors (the so-called TPP stimulation) results in a specific molecular pattern and phenotype that departs from the well-established classical M1 and alternative M2 activation state axis (Xue et al., 2014). In particular, the cell-surface markers CD25, CD14 and CD23 as well as the IL1α cytokine and, to a lesser extent, the CXCL5 chemokine were found to be induced in a TPP-specific condition (Xue et al., 2014). Remarkably, elevated levels of both TNFα and PGE_2 have been documented in the *substantia nigra* of PD patients suggesting that these inflammatory mediators might act in concert with TLR-activating pathological αSYN aggregates to drive microglial cell polarization toward a specific disease phenotype. Therefore, in an effort to better model chronic-type PD innate immune response, we sought to integrate these disease-relevant inflammatory cues together with αSYN fibrils, the presumably primary pathological trigger.

We first tested whether microglial cells would respond similarly to peripheral macrophages upon chronic-type inflammatory stimulation as previously described (Xue et al., 2014). Indeed, whilst peripheral macrophages and microglia share origin in the yolk sac, microglia are an ontogenetically distinct cell population and so their responsiveness to chronic-type inflammatory stimulation may not exactly mirror that of their macrophage relatives (Ginhoux et al., 2010). We thus investigated the expression of TPP-induced immune markers in microglial cells exposed to a combination of TNFα (800 UI/ml), PGE_2 (1µg/ml) and the TLR2 agonist Pam3CSK4 (Pam3C; 1µg/ml) as compared to cells stimulated with conditions linked to M1 (IFNγ; 20 ng/mL) or M2 (IL4; 10 ng/mL) polarization. Immunostaining for CD25 revealed that unlike peripheral macrophages, microglial cells not only express high basal level of this cell-surface marker but also display unchanged expression under M2 and TPP stimulation, and down-regulation under M1 polarization (Figure 2A). Similarly, whereas IL1α was specifically induced in TPP-stimulated macrophages (Xue et al., 2014), it was only increased in M2-polarized (IL4-treated) microglial cells (Figure 2B). Finally, TPP-exposed microglial cells produced and released as much CXCL5 as IL4-treated cells, a result contrasting with the upregulation of this

chemokine in both IFNγ- and TPP-stimulated human macrophages (Figure 2B). Of note, poor or degraded biological activity of recombinant IFNγ was unlikely to account for the apparent unresponsiveness of microglial cells to IFNγ-induced CXCL5 since this treatment efficiently stimulated the intracellular production of reactive oxygen species (ROS) as a consequence of NADPH-oxidase activation (Figure 2C). Altogether, these data show that microglial cells feature distinct TPP-associated gene regulation compared to peripheral macrophages.

We next investigated microglial cell response to chronic-type inflammatory stimulation by implementing PD patients-derived αSYN fibrils (F^{PD}) in the treatment cocktail assuming that F^{PD} would efficiently bind and activate microglial TLRs as demonstrated for αSYN fibrils made *de novo* (Choi et al., 2020; Fellner et al., 2013; Gustot et al., 2015; Lim et al., 2016; Scheiblich et al., 2021). Using ELISA assay, we found that unlike LPS and F^{PD}, TNFα and PGE_2, alone or in combination (TP), were ineffective in stimulating TNFα, IL6, IL1β and IL10 release after 48 hours of treatment (Figure 3A and B). Remarkably, co-treatment of F^{PD}-exposed cells with TNFα and PGE_2 (TPF^{PD} stimulation) significantly curtailed cytokine released compared to F^{PD} alone suggesting that chronic-type inflammatory stimulation is associated with significant but less intensive inflammatory state. To determine whether TPF^{PD} stimulation is associated with an overall reduced inflammatory grade of microglial cells, we measured and compared intracellular ROS levels following the different treatments. Figure 3C shows that, unlike cytokine production/release, TP did not mitigate F^{PD}-induced ROS generation in microglial cells. To expand further on the inflammatory properties associated with TPF^{PD} stimulatory condition, we analyzed microglial glutamate release in these conditions. We observed that unlike cytokine (decrease) and ROS (unchanged) production, TPF^{PD} treatment was associated with a significant increase in extracellular glutamate level compared to F^{PD} treatment alone (Figure 3D). Overall, our data show that upon chronic-type inflammatory stimulation, microglial cells adopt a non-conventional phenotype as compared to the classical M1 pro-inflammatory state of activation.

Chronic-type inflammatory stimulation of microglia is associated with a specific genomic signature.

The above data showing specific inflammatory features of microglia subjected to TPF^{PD} stimulation might point out to unique molecular pathway engagement and transcriptional programming as previously exemplified in peripheral macrophages (Xue et al., 2014). To gain insight into the molecular signature of such inflammatory polarization, we conducted unbiased transcriptomic analysis through RNA-sequencing (RNA-seq) performed on non-stimulated cells (NSC), LPS-polarized cells taken as a reference of M1 pro-inflammatory state, and TPF^{PD}-activated microglia. To examine the effect of stimulation, we initially performed unsupervised principal component analysis (PCA). As expected, the samples separated well by activation status (NSC vs stimulated) on the first principal component but also by type of stimulation (LPS vs TPF^{PD}), that was driving the second component of the variability (Figure 4A). By using differentially expressed genes (DEGs; log2FC > 0.5, false discovery rate [FDR] adjusted *P* value < 0.05) between TPF^{PD}, M1 (LPS) and NSC we identified 554 upregulated and 456 downregulated genes in TPF^{PD}-exposed cells. Unsupervised cluster analysis of the top 413 DEGs (by *P*-value) showed a striking difference between the transcriptomes of M1-polarized and TPF^{PD}-treated microglia (Figure 4B). To get insights on how differential gene regulation translate into pathway modulation we first processed expression data with the Pathifier algorithm that transforms gene-level information into pathway-level records (Drier et al., 2013). Principal component analysis of newly generated pathway-related dataset indicates that both stimulation and type of stimuli drive strong pathway variability (Figure 4C). To document in details pathways and biological functions altered by chronic-type inflammatory stimulation, we performed pathway enrichment (KEGG) and gene ontology (GO) term analysis. We found that among the most significantly enriched KEGG pathways in TPF^{PD}-stimulated cells were ribosome biogenesis, glutathione metabolism, steroid biosynthesis, spliceosome, ferroptosis and RNA transport (Figure 4D). Results from GO analysis confirmed pathway enrichment data for the most part. Yet, they additionally revealed other features related to regulation of inflammatory response and primary metabolic and lipid processes (Figure S2). Of note, increased glutathione metabolism in TPF^{PD}-stimulated microglial cells might be possible in condition of high

cysteine supply and glutamate level provided that the expression and/or activity of the rate-limiting enzymes glutathione cysteine ligase (GCL) and glutathione synthase (GSS) are increased. One possible mechanism that could rise microglial cysteine levels upon inflammatory stimulation is the activation of xCT, a transmembrane cystine-glutamate exchange transporter coded by the *Slc7a11* gene (Lewerenz et al., 2013). Remarkably, both *Slc7a11*, *Gss* and *Gcl* genes (*Gclc* and *Gclm*) were found to be among the most upregulated genes in TPF^{PD}-stimulated cells (Figure 4E). Increased *Slc7a11* gene expression in TPF^{PD}-stimulated microglia is in line with the higher capacity of these cells in releasing glutamate (Figure 3C).

Another interesting observation is the apparent link of TPF^{PD} stimulation with ferroptosis. Ferroptosis is a type of redox-driven programmed cell death process distinct from classical apoptosis. It might emerge because of uncontrolled iron metabolism, lipid peroxidation and thiol regulation, three processes that are commonly found in the pro-inflammatory environment. Since in our experimental conditions TPF^{PD}-stimulation does not induce microglial cell death (Figure S3), it is likely that genes involved in iron metabolism contributed to the ferroptosis term in our pathway enrichment list. Indeed, we found that iron transport- and storage-related genes including *Tfrc*, *Slc39a14* and *Fth1* (coding for the Transferrin receptor, the zinc and non-transferrin-bound iron transporter Zip14, and the Ferritin heavy chain, respectively) were strongly and differentially upregulated in TPF^{PD}-treated cells (Figure 4E). Genes coding for the divalent metal transporter 1 (DMT1) and the iron extruder Ferroportin (*Slc11a2* and *Slc40a1*) were similarly expressed in LPS- and TPF^{PD}-exposed cells (Figure 4E). Overall, our data suggest differences in microglial iron handling in two distinct inflammatory conditions.

To validate our transcriptomic data, we performed qPCR expression analysis of gene candidates using total RNA isolated from microglial cells exposed or not to LPS and TPF^{PD} in an independent experiment. We confirmed the differential expression of *Gss*, *Gclc, Gclm* and *Slc7a11* in TPF^{PD}-treated cells as compared to non-stimulated and LPS-exposed microglia (Figure 4F). Likewise, iron metabolism-related

genes (*Tfrc*, *Slc39a14*, *Fth1*, *Slc11a2* and *Slc40a1*) showed similar expression changes as identified in transcriptomic analysis (Figure 4F). Together, we have identified genes and pathways that define polarized microglia upon TPF^{PD} chronic-type inflammatory condition.

TPF^{PD}-related chronic-type inflammatory stimulation of microglia is associated with M1-related metabolic changes.

The above transcriptome-based analysis revealed pathway enrichment linked to metabolic processes. It is now well established that immune activation rapidly and substantially enhances metabolic outputs that in turn regulate immune responses (Rodríguez-Prados et al., 2010). For instance, in macrophages, including microglia, the M1 phenotype polarization is accompanied by a shift from oxidative phosphorylation to aerobic glycolysis for energy production (Orihuela et al., 2016). To further document TPF^{PD}-associated metabolic changes in microglia, we performed untargeted metabolomic analysis under the same experimental conditions as above.

Our results show significant alterations in the level of 248 metabolites in TPF^{PD}-treated cells. Indeed, hierarchical clustering analysis of metabolite datasets and heatmap generation (Figure 5A) showed important differences between non-stimulated cells and microglia exposed to either LPS or TPF^{PD}. The metabolome profile of TPF^{PD}-activated cells displays only subtle differences with that of LPS-treated microglia. Of the 248 metabolites showing significant changes, only 28 were annotated in databases. Unsupervised cluster analysis of these 28 known metabolites confirms the close relationship between the two inflammatory conditions (Figure 5B). In particular, both stimulations resulted in decreased α-ketoglutarate/succinate and fumarate/succinate ratios indicative of tricarboxylic acid (TCA) cycle break and metabolic switch from oxidative phosphorylation to glycolysis as previously reported (Angajala et al., 2018). Hence, these data suggest that from a respiratory point of view, TPF^{PD}-polarized microglia behave as classical pro-inflammatory M1 cells. Moreover, and despite that TPF^{PD}-polarized microglia releases larger amount of glutamate than LPS-activated cells (Figure 3C), these two inflammatory

stimulations are characterized by comparable increase in glutamate and glutathione disulfide levels (Figure 5C). Hence, our data show that metabolic changes associated with M1 and TPF^{PD} microglial polarization are closely related.

Conserved TPF^{PD}-specific induction of Tfrc and Slc7a11 gene expression in human induced microglial-like cells.

Integration and comparison of human and murine transcriptome data sets indicate both divergent and conserved gene expression regulation upon inflammatory stimulation between species (Galatro et al., 2017). Our comparative study of TPP-induced inflammatory markers in mouse microglial cells clearly illustrates such divergence pointing out cell-type and/or species specificity (Figure 2). To elaborate further on human relevance of our data generated with mouse microglia, we prepared and used induced-microglia-like cells (iMGs) that were differentiated from human monocytes isolated from healthy donors (Ohgidani et al., 2015). Successful differentiation of monocytes into iMGs was controlled by investigating the expression of the CCR2 and CX3CR1 chemokine receptors. As shown in Figure 6A, monocyte differentiation into iMGs was accompanied by a significant increase in the CX3CR1/CCR2 ratio indicating that differentiated cells acquired a macrophage-/microglia-like phenotype (Mizutani et al., 2012). After 24 days of differentiation, iMGs were exposed or not (NSC) to LPS, F^{PD} or TPF^{PD} at concentrations equivalent to those used for mouse microglia experiments and then collected after 48 hours of activation for assessment by qPCR of candidate genes. We found that, similar to mouse microglial cells, TPF^{PD} chronic-type inflammatory stimulation of iMGs results in specific upregulation of *Tfrc* and *Slc7a11* compared to LPS or F^{PD} treatments (Figure 6B). Likewise, although not statistically significant, a clear trend in increased expression of *Slc11a2* was observed in both LPS and TPF^{PD} conditions. By contrast, *Gclm* was found to be equally induced in LPS- and TPF^{PD}-exposed cells but not in F^{PD} alone stimulatory condition. Interestingly, TPF^{PD} stimulation specifically induces marked upregulation of *Tlr2* in iMGs compared to LPS and F^{PD} in contrast to what we observed

in mouse microglial cells. Moreover, while *Tlr4* expression was reduced upon LPS and F^{PD} treatments compared to control cells (NSC), it remained unchanged in TPF^{PD} condition suggesting that regulation of TLRs expression in human microglia highly depends on the type of inflammation and inflammatory stimuli. Together, our data support previous findings showing species-dependent gene regulation in macrophages and demonstrate conserved TPF^{PD}-associated *Tfrc* and *Slc7a11* gene regulation between mouse and human microglia. They further highlight that TPF^{PD}-stimulated microglia may acquire a unique phenotype characterized by higher iron retention capacity and glutamate release.

Chronic-type inflammatory stimulated microglia exhibits xCT-dependent neurotoxic activity on dopaminergic neurons.

Our molecular and phenotypic analysis of microglial cells stimulated by chronic-type inflammatory cues revealed that cells under such activation are particularly prone to release high amount of glutamate compared to classically activated (M1) pro-inflammatory microglia. Such peculiar effector function of TPF^{PD}-activated cells may be detrimental for dopaminergic neurons that are particularly vulnerable to glutamate-induced excitotoxicity (Wang et al., 2020). Therefore, we next sough to test this hypothesis using a model system of microglia-conditioned medium (MCM) transfer onto midbrain neuronal cultures. In preliminary experiments, we observed that LPS were ineffective in inducing glutamate release from microglial cells grown in Nba and Nba-based ACM supplemented or not with 200µM L-cystine suggesting that DMEM-based medium was strictly necessary for inflammatory stimulation of microglia (data not shown). Likewise, we found that DMEM-based medium (either supplemented with 1% FBS or B27/N2 mix or DMEM-based ACM) was incompatible with proper midbrain neuron maturation and viability over 7 days of culture. On the other hand, neurons grown in Nba-based ACM for 7 days could stand partial medium change (up to 50%, v/v) with microglial-compatible DMEM-based ACM without any sign of damage 24 hours later (data not shown). Therefore, we tested and compared dopaminergic neuron (grown in Nba-based ACM) viability 24 hours after the

transfer of MCM (30%, v/v) from F^{PD}- and TPF^{PD}-stimulated microglia (grown in DMEM-based ACM) (Figure 7A). To prevent any possible direct neuronal effect of the inflammatory stimulating factors (F^{PD} or TPF^{PD}), we set up a washout step after microglial inflammatory stimulation for 6 hours and let activated microglial cells for 24 hours in fresh DMEM-based ACM (Figure 7A). At this time, MCM from F^{PD}- or TPF^{PD}-stimulated microglia display higher glutamate levels than that from NSC condition (Figure 7A). Under such experimental setup, we found that TPF^{PD}-stimulated MCM induced significantly more TH+ dopaminergic neuron loss compared to F^{PD} stimulation suggesting that chronic-type inflammatory stimulation drives microglia toward a more aggressive phenotype than classically activated M1 cells (Figure 7B and C). Furthermore, we observed that the rate of TH+ neuronal loss was strongly correlated with MCM glutamate content suggesting that xCT-dependent glutamate release and glutamate-induced excitotoxicity may underline key neurotoxic mechanisms supported by chronic-type inflammatory microglial cells (Figure 7D). To test this hypothesis, we exposed F^{PD}- and TPF^{PD}-stimulated microglial cells to the xCT inhibitor Sulfasalazine (250 µM) during 24 hours after the washout step and transferred the resulting MCM onto midbrain neurons. Sulfasalazine treatment of stimulated microglial cells completely abrogated MCM-associated dopaminergic toxicity suggesting an essential role of xCT function in the neurotoxic activity of chronic-type inflammatory microglial cells (Figure 7C). Finally, to establish that TPF^{PD}-activated microglial cells were likely inducing dopaminergic cell death through glutamate-dependent excitotoxic mechanisms, we treated MCM-exposed midbrain cultures with MK-801 (2µM), an inhibitor of the glutamate receptor NMDAR (*N*-methyl-D-aspartate receptor). As shown in Figure 7C, MK-801 treatment conferred full neuroprotection against MCM-associated damage indicating that chronic-type inflammatory microglial cells efficiently induce excitotoxic dopaminergic neuronal death.

Discussion

In this study, we investigated the inflammatory properties of PD patients-derived αSYN fibrils on microglial cells and explored their capacity to induce a unique immune response when combined with TNFα and Prostaglandin E_2 (PGE_2), two inflammatory cues commonly elevated in chronic inflammatory diseases and in PD patients. We found that fibrils derived by PMCA from PD patients hold stronger inflammatory potency than recombinant human αSYN fibrils generated *de novo* in cultured mouse microglia suggesting a relationship between the structure of aggregated αSYN and macrophage immune response. Importantly, the inflammatory response elicited by PD patients-derived αSYN fibrils on microglia was profoundly modulated in the presence of TNFα and PGE_2 with lower cytokine but higher glutamate release responsiveness. This "chronic-type" inflammatory stimulation resulted in a specific molecular reprogramming of microglial cells departing from classically activated and pro-inflammatory M1 microglia and characterized by seemingly higher iron retention and excitotoxic capacities.

Microglia, the most abundant resident macrophages of the central nervous system (CNS), play important roles for the maintenance of tissue homeostasis (Colonna & Butovsky, 2017; Prinz et al., 2019; Ransohoff & Perry, 2009). Yet, upon neuronal injury, they get rapidly activated and mount an inflammatory response that, if persisting, can prove neurotoxic (Bodea et al., 2014; Donat et al., 2017; Lull & Block, 2010). In PD, protracted microglial cell activation is a neuropathological characteristic that accompanied neurodegeneration and deposition of pathological αSYN (Ouchi et al., 2009). Protein aggregates are a common feature of several ageing-related neurodegenerative diseases and have been linked to microglial cell activation and ensuing inflammatory response through ligation of pattern recognition receptors (PRRs) (Heneka et al., 2015). Mounting evidences suggest that αSYN aggregates, which are eventually released from neurons as part of the prion-like propagation mechanism of the synucleinopathy across neuronal networks, are a major pathological trigger of microglial activation and inflammation in PD (Choi et al., 2020; Daniele et al., 2015). Yet, the importance of the respective PRRs

in this process is still a subject of debate. While some authors pointed out a key role of TLR2, others found that TLR4 may be important as well (Codolo et al., 2013; Fellner et al., 2013; Feng et al., 2019; C. Kim et al., 2013). The discrepancy between these results is likely to stem from the type and purity of αSYN assemblies used in different studies. Recently, using distinct well-characterized recombinant human αSYN assemblies generated *de novo*, we found that TLR2 and TLR5, but not TLR4, were indispensable for monomeric and oligomeric αSYN to efficiently activate the NOD-like receptor pyrin domain containing 3 (NLRP3) inflammasome and IL1β release from microglial cells (Scheiblich et al., 2021). Equal concentrations of αSYN fibrillar polymorphs were unable to evoke IL1β release during the same stimulation period (Scheiblich et al., 2021). Thus, these data strongly suggest that the structural characteristics of αSYN assemblies are a major determinant of their innate immunological properties. In support of this view, we showed here that fibrils derived from PD patients (F^{PD}) elicited a greater inflammatory response than fibrils assembled *de novo* but a lower one compared to those amplified from DLB patients (F^{DLB}). Strikingly, whereas F^{S} (2µM) was unable to induce IL1β release in unprimed microglial cells (Scheiblich et al., 2021), we found that lower concentrations of F^{PD} (1.5µM) induced robust IL1β response (Figure 3B). Since F^{PD} are structurally different from F^{DLB} and F^{S} (Guerrero-Ferreira et al., 2019; Burger et al., 2021), our data further support the view that αSYN assemblies with different structures hold distinct inflammatory potency on microglial cells. The structure-function relationship depicted here for microglia-associated immune response is reminiscent to that documented for neuronal deposition of pathological αSYN and toxicity (Shahnawaz et al., 2020; Van der Perren et al., 2020). Indeed, we recently reported that structurally distinct αSYN fibrils assembled *de novo* or derived from PD, DLB and MSA patients results in different synucleinopathy-associated characteristics and toxicity in cultured cells and after inoculation in rodents brain (Rey et al., 2019; Shrivastava et al., 2020; Van der Perren et al., 2020). The structural differences between patient-derived and *de novo* assembled fibrils may originate from the different surfaces distinct fibrillar polymorphs expose to the solvent that define their differential binding to cell surface proteins and seeding propensity in cells (Shrivastava et al., 2020; Landureau et al., 2021). Hence, it is likely that the capacity of the F^{PD}

polymorph to evoke stronger inflammatory response than its recombinant relative might be linked to its ability either to bind with higher affinity to innate immune receptors or to activate different type of receptors. Yet, the binding capacity of F^{PD} to different TLRs or other innate immune receptors remains to be established.

A major contribution of our study is the demonstration that F^{PD}-induced microglial inflammatory response is profoundly altered when associated with the pro-inflammatory cytokine TNFα and PGE_2, an arachidonic acid-derived lipid modulator of inflammation. As part of this demonstration, we further showed that under such combinatory stimulation (so called TPF^{PD}), microglial cells engage a distinct molecular program as compared to LPS-induced pro-inflammatory M1 cells. TNFα and PGE_2, are common immune-related factors featuring chronic inflammatory conditions (Aoki & Narumiya, 2012; Balkwill, 2009). In PD, a neurodegenerative disease associated with chronic neuroinflammatory processes, the expression level of TNFα and the PGE_2-producing enzyme cyclooxygenase 2 (COX2) were shown to be increased (Mattammal et al., 2002; Mogi et al., 1994; Teismann et al., 2003). Moreover, compelling experimental evidences support an independent pathogenic role of these inflammatory factors suggesting that besides being part of a large panel of effector molecules derived from activated glial cells or injured neurons, these inflammatory cues are instrumental in neuronal cell death (Tansey & Goldberg, 2010; Teismann et al., 2003). Hence, although αSYN aggregates are considered as a primary and master disease-associated inflammatory trigger in PD, other immune-related factors, as part of a global network of neuroinflammatory processes (Hirsch & Hunot, 2009), may play a significant contribution in regulating microglial-associated inflammation and toxicity. Indeed, it is now well established that microglial cells, and tissue macrophages in general, are very plastic and can adopt a great variety of activation phenotype associated with specific functions. Analysis and network modeling of transcriptional regulation during human macrophage activation elicited by a diverse set of stimuli has clearly established a spectrum model of macrophage activation reassessing and extending the prevailing M1 (pro-inflammatory or classically activated) versus M2 (anti-inflammatory or alternatively activated) polarization model (Xue et al., 2014). In

particular, macrophages exposed in a combinatory mode to chronic inflammation-associated factors TNFα, PGE_2, and TLR2 ligands (the so called "TPP" stimulation) feature specific molecular modules not found in IFNγ- (M1) or IL4- (M2) stimulated cells and, consequently expressed specific cell surface markers and cytokines. Yet, the finding obtained in human macrophages might not be totally transposed to murine microglia. Indeed, we found that the regulation of TPP-specific markers (CD25, CXCL5 and IL1α) in mouse microglial cells was markedly different from human macrophages highlighting important macrophage identity- and/or species-related specificity as previously reviewed (Locati et al., 2020). Yet, despite these differences, our results clearly show that, as documented in human macrophages, chronic-type inflammatory stimulation of microglia is associated with a specific transcriptional reprogramming departing from classically activated M1 cells. Interestingly, some of the molecular pathways characterizing this chronic-type inflammatory stimulation were consistent with functional properties defined before. In particular, the finding that TPF^{PD}-stimulated cells feature higher xCT-coding *Slc7a11* gene expression is consistent with the enhanced responsiveness of these cells to glutamate release. Importantly, a similar up-regulated expression of *Slc7a11* was detected in human microglial-like cells (iMGs) exposed to TPF^{PD} arguing that this chronic-type inflammatory-associated regulation is conserved across mouse and human species. While releasing glutamate, the xCT antiporter internalizes cystine which is needed for glutathione synthesis. In line with this scenario, we further observed that TPF^{PD}-polarized microglial cells are characterized by the specific up-regulation of several genes (*Gss, Gclc* and *Gclm*) coding for rate-limiting enzymes involved in glutathione synthesis. The cystine-glutamate antiporter xCT has been previously shown to contribute to the pro-inflammatory phenotype of primary microglial cells and to be involved in amyotrophic lateral sclerosis (ALS)- and Alzheimer's disease-related pathogenesis (Mesci et al., 2015; Qin, 2006). In particular, a decreased production of specific microglial pro-inflammatory/neurotoxic factors including nitric oxide, TNFα and IL6 was observed in xCT-deleted microglial cells exposed to LPS (Mesci et al., 2015). Our data showing decreased TNFα and IL6 production concomitant with increased *Slc7a11* gene expression and glutamate release in TPF^{PD}-stimulated microglia suggest that the regulatory

mechanisms of pro-inflammatory cytokine expression by xCT differ between different microglial activation states. Hence, the importance of our finding in the context of PD-related neuroinflammation stem to the fact that glutamate has the potential to generate low-level excitotoxic insults (Lavaur et al., 2017) that may contribute to neuronal cell death (Ambrosi et al., 2014). In line with this, we provide compelling evidence that xCT-dependent glutamate release from chronic-type inflammatory microglia results in NMDAR over activation-mediated excitotoxic dopaminergic cell death. In the field of PD, previous studies have reported an increased in xCT expression upon injection of 6-hydroxydopamine (6-OHDA) in hemi-Parkinson rats (Massie et al., 2008). Moreover, neuroprotection has been documented in xCT-null mice injected with 6-OHDA (Massie et al., 2011). Yet, inhibition of xCT by gene targeting does not protect mice from MPTP-induced dopaminergic cell loss (Bentea et al., 2015). Thus, although debated, the role of xCT in PD pathogenesis is still an open question. Of note, its pathogenic role has never been investigated in PD animal models featuring degenerative synucleinopathy.

Apart from glutathione metabolism, identification of TPF^{PD}-specific ferroptotic pathway in our KEGG analysis was surprising given the fact that we did not observe microglial cell death upon exposure to TPF^{PD}. Moreover, it has been documented that macrophages display significant defiance against ferroptotic stimulation and death in particular when polarized into classically activated M1 state (Kapralov et al., 2020). Yet, as part of the set of genes building this pathway, we found that TPF^{PD} stimulation was associated with elevated expression of iron-related transport proteins coupled with increased intracellular iron-storage capacity. Increased iron retention is a well-known function of inflammatory macrophages that serves as a primary defense mechanism against pathogens through extracellular iron starvation. Yet, macrophage iron uptake fulfill additional important role as it is an essential metal that fine-tunes metabolic changes associated with immune activation thereby contributing directly to macrophage function and plasticity (Pereira et al., 2019). Previous report indicated that M1-type microglia preferentially acquire iron from non-Transferrin-bound iron (NTBI) whereas M2 polarized cells promote TBI uptake (McCarthy et al., 2018). Our data are consistent with this general scheme since LPS-induced microglial activation was associated with concomitant

increased and decreased gene expression of *Slc11a2* (coding for the divalent metal transporter 1; DMT1) and *Tfrc* (coding for the Transferrin receptor), respectively. Remarkably, however, TPF^{PD}-stimulated cells were characterized by increased gene expression in both *Slc11a2* and *Tfrc* showing a unique iron transport phenotype featuring both M1 and M2 properties. Their presumably higher iron retention capacity as compared to LPS-polarized cells is further supported by the specific upregulation of the gene coding for ZIP14 (*Slc39a14*), a complex broad-scope metal-ion transporter of zinc and non-transferrin-bound iron. Coupled with increased iron uptake capacity, TPF^{PD}-polarized microglia further display high decrease in *Slc40a1* gene expression (coding for the iron extruder Ferroportin) as well as robust increase in *Fth1* coding for the iron storage Ferritin heavy chain. As for *Slc7a11* gene regulation, TPF^{PD}-elicited *Tfrc* and *Slc11a2* upregulated gene expression was conserved in human iMGs comforting the human relevance of our finding. Altogether, these data suggest that microglial cells polarized under TPF^{PD}-associated chronic-type inflammation feature both M1- and M2-associated iron metabolism regulation and propose that they might be particularly iron retentive compared to M1 and M2 inflammatory cells. Relevant to our finding, is the recent observation that iron accumulate prematurely and preferentially in microglial cells over dopaminergic neurons in a non-human primate model of degenerative synucleinopathy induced by intranasal administration of human αSYN preformed fibrils (PFFs) (Guo et al., 2021).

It is now well established that in response to environmental cues, such as inflammatory stimuli, microglia shift their metabolism as part of an adaptative mechanism that drives specific effector functions. In particular, it has been documented that TLR-related pro-inflammatory stimulation (e.g. LPS) induces a metabolic shift from oxidative phosphorylation to glycolysis, a phenomenon known as the Warburg effect initially characterized in tumor cells (Orihuela et al., 2016; Warburg, 1956). Consistent with this, we found that LPS stimulation of microglia resulted in a decreased α-ketoglutarate/succinate and fumarate/succinate ratios indicative of tricarboxylic acid (TCA) cycle break. Importantly, the immune response evoked by TPF^{PD} stimulation was associated with similar metabolic changes suggesting that from a respiratory point of view this chronic-type inflammation

share common features with classical M1-polarized cells. Surprisingly, despite the fact that TPF^{PD}-stimulated cells release more glutamate than LPS-exposed cells, we observed similar intracellular levels of glutamate between these two inflammatory conditions. Therefore, we posit that the higher capacity of TPF^{PD}-polarized cells to extrude glutamate is likely to be linked to increased expression of xCT rather than enhanced glutamate synthesis pathway activity.

In summary, we documented that PD patients-derived αSYN fibrils hold robust inflammatory properties on microglial cells. Furthermore, we showed that combined with TNFα and PGE_2, this disease-associated αSYN polymorph polarizes microglia into a specific "chronic-type" inflammatory activation state and phenotype featuring both M1- and M2-related traits and exhibiting overwhelming neurotoxic activities. Of note, composed M1/M2 polarization assignment has been previously documented in animal models of traumatic brain injury, ALS and glioma-associated neurological disease suggesting that our model system may, in part, recapitulate more closely some of the complex innate inflammatory mechanisms *in vivo* (Chiu et al., 2013; Kim et al., 2016; Morganti et al., 2016; Szulzewsky et al., 2015). In support of this view, we could identify few overlaps between TPF^{PD}-stimulated microglia *in vitro* and the recently characterized disease-associated microglia (DAM) isolated from mouse models of Alzheimer's disease and ALS (Keren-Shaul et al., 2017). In particular, few of the genes assigned to DAMs were found to be differentially expressed in TPF^{PD}-polarized microglia including *B2m*, *Lyz2* and *Cst7* (data not shown). Nonetheless, global gene expression overlap between the DAM's transcriptome and those from LPS- or TPF^{PD}-derived cells remained modest (53 and 50 genes, respectively) highlighting significant differences in genomic expression patterns between *in vitro* and *in vivo* microglia cells as previously reported (McFarland et al., 2021). Yet, although we are well aware that the model described here is not a phenocopy of activated microglial cells in the brain of PD patients, it may serve as a general framework to explore and understand the disease-associated mechanisms underlying complex inflammatory-induced signal integration that shape microglial cell activation and function. Hence, such knowledge should facilitate the identification of new potential targets for therapeutic intervention and may lead to the discovery of biomarkers.

Acknowledgments

This work was supported by funding from the Joint Program on Neurodegenerative Diseases (JPND) to S.H. and R.M. (01ED1603). S.H. received further funding from the Sanofi Innovation Awards - Europe Program Funding Award (2018 iAward). C.Y. and P.B. were supported by the Neuroscience School of Paris foundation (ENP), and the French Ministry of Higher Education and Research as well as the Association France Parkinson, respectively. The research leading to these results has received funding from the program "Investissements d'Avenir" ANR-10- IAIHU-06 and ANR-11- INBS-0011 – NeurATRIS: Translational Research Infrastructure for Biotherapies in Neurosciences.

The authors would like to thank Prof. Jean-Christophe Corvol and the Clinical Investigation Center for Neurosciences of the Pitié-Salpêtrière Hospital (CIC 1421, Paris, France) for their help in collecting human blood samples. We are indebted to Prof. Steve Gentleman at the Neuropathology Unit, Division of Brain Sciences, Department of Medicine, Imperial College London for providing us with PD and DLB patient brain tissues. We also thank Dr. Luc Bousset for his invaluable advice in preparing αSyn assemblies *in vitro*. Part of this work was carried out on the CELIS cell culture, the iGenSeq and the Data and Analysis core facilities of ICM. We gratefully acknowledge Yannick Marie, Justine Guegan and David Akbar for helpful discussions and advice on technical aspects of the project. We would also like to thank Farid Ichou and Maha Ponnaiah from the ICANalytics core facility (ICAN Institute, Salpêtrière Hospital, Paris France) for their help regarding sample preparation and processing for metabolomics and bioinformatics data analysis and Tracy Bellande for expert technical assistance. Finally, we thank the patients and caregivers for their participation and contribution to this study.

Author contributions

C.Y and S.H. designed all experiments; C.Y., L.G., J.S-D and P.B. performed experiments and analyzed data with the assistance of P.P.M. and S.H.; A.F. and R.M. generated and characterized all α-Synuclein assemblies and provided advice; and C.Y. and S.H. wrote the manuscript with input from all co-authors.

Declaration of interests

The authors declare that there is no conflict of interest regarding the experimental part of this study.

References

Ambrosi, G., Cerri, S., & Blandini, F. (2014). A further update on the role of excitotoxicity in the pathogenesis of Parkinson's disease. *Journal of Neural Transmission*, *121*(8), 849–859. https://doi.org/10.1007/s00702-013-1149-z

Angajala, A., Lim, S., Phillips, J. B., Kim, J.-H., Yates, C., You, Z., & Tan, M. (2018). Diverse roles of mitochondria in immune responses: novel insights into immuno-metabolism. *Frontiers in Immunology*, *9*, 1605. https://doi.org/10.3389/fimmu.2018.01605

Aoki, T., & Narumiya, S. (2012). Prostaglandins and chronic inflammation. *Trends in Pharmacological Sciences*, *33*(6), 304–311. https://doi.org/10.1016/j.tips.2012.02.004

Balkwill, F. (2009). Tumour necrosis factor and cancer. *Nature Reviews Cancer*, *9*(5), 361–371. https://doi.org/10.1038/nrc2628

Benjamini, Y., & Hochberg, Y. (1995). Controlling the False Discovery Rate: A Practical and Powerful Approach to Multiple Testing. *Journal of the Royal Statistical Society. Series B (Methodological)*, *57*(1), 289–300. JSTOR.

Bentea, E., Sconce, M. D., Churchill, M. J., Van Liefferinge, J., Sato, H., Meshul, C. K., & Massie, A. (2015). MPTP-induced parkinsonism in mice alters striatal and nigral xCT expression but is unaffected by the genetic loss of xCT. *Neuroscience Letters*, *593*, 1–6. https://doi.org/10.1016/j.neulet.2015.03.013

Bodea, L.-G., Wang, Y., Linnartz-Gerlach, B., Kopatz, J., Sinkkonen, L., Musgrove, R., Kaoma, T., Muller, A., Vallar, L., Di Monte, D. A., Balling, R., & Neumann, H. (2014). Neurodegeneration by Activation of the Microglial Complement-Phagosome Pathway. *Journal of Neuroscience*, *34*(25), 8546–8556. https://doi.org/10.1523/JNEUROSCI.5002-13.2014

Bousset, L., Pieri, L., Ruiz-Arlandis, G., Gath, J., Jensen, P. H., Habenstein, B., Madiona, K., Olieric, V., Böckmann, A., Meier, B. H., & Melki, R. (2013). Structural and functional characterization of two alpha-synuclein strains. *Nature Communications*, *4*(1), 2575. https://doi.org/10.1038/ncomms3575

Brundin, P., Melki, R., Kopito, R. (2010) Prion-like transmission of protein aggregates in neurodegenerative diseases. *Nat Rev Mol Cell Biol*, 11(4):301-7. doi: 10.1038/nrm2873.

Burger, D., Fenyi, A., Bousset, L., Stahlberg, H., Melki, R. (2021) Cryo-EM structure of alpha-synuclein fibrils amplified by PMCA from PD and MSA patient brains. bioRxiv, 451588; doi: https://doi.org/10.1101/2021.07.08.451588

Chen, E. Y., Tan, C. M., Kou, Y., Duan, Q., Wang, Z., Meirelles, G. V., Clark, N. R., & Ma'ayan, A. (2013). Enrichr: Interactive and collaborative HTML5 gene list enrichment analysis tool. *BMC Bioinformatics*, *14*(1), 128. https://doi.org/10.1186/1471-2105-14-128

Chiu, I. M., Morimoto, E. T. A., Goodarzi, H., Liao, J. T., O'Keeffe, S., Phatnani, H. P., Muratet, M., Carroll, M. C., Levy, S., Tavazoie, S., Myers, R. M., & Maniatis, T. (2013). A Neurodegeneration-Specific Gene-Expression Signature of Acutely Isolated Microglia from an Amyotrophic Lateral Sclerosis Mouse Model. *Cell Reports*, *4*(2), 385–401. https://doi.org/10.1016/j.celrep.2013.06.018

Choi, I., Zhang, Y., Seegobin, S. P., Pruvost, M., Wang, Q., Purtell, K., Zhang, B., & Yue, Z. (2020). Microglia clear neuron-released α-synuclein via selective autophagy and prevent neurodegeneration. *Nature Communications*, *11*(1), 1386. https://doi.org/10.1038/s41467-020-15119-w

Ciofani, M., Madar, A., Galan, C., Sellars, M., Mace, K., Pauli, F., Agarwal, A., Huang, W., Parkurst, C. N., Muratet, M., Newberry, K. M., Meadows, S., Greenfield, A., Yang, Y., Jain, P., Kirigin, F. K., Birchmeier, C., Wagner, E. F., Murphy, K. M., … Littman, D. R. (2012). A Validated Regulatory Network for Th17 Cell Specification. *Cell*, *151*(2), 289–303. https://doi.org/10.1016/j.cell.2012.09.016

Codolo, G., Plotegher, N., Pozzobon, T., Brucale, M., Tessari, I., Bubacco, L., & de Bernard, M. (2013). Triggering of Inflammasome by Aggregated α–Synuclein, an Inflammatory Response in Synucleinopathies. *PLoS ONE*, *8*(1), e55375. https://doi.org/10.1371/journal.pone.0055375

Colonna, M., & Butovsky, O. (2017). Microglia Function in the Central Nervous System During Health and Neurodegeneration. *Annual Review of Immunology*, *35*(1), 441–468. https://doi.org/10.1146/annurev-immunol-051116-052358

Cottret, L., Frainay, C., Chazalviel, M., Cabanettes, F., Gloaguen, Y., Camenen, E., Merlet, B., Heux, S., Portais, J.-C., Poupin, N., Vinson, F., & Jourdan, F. (2018). MetExplore: Collaborative edition and exploration of metabolic networks. *Nucleic Acids Research*, *46*(W1), W495–W502. https://doi.org/10.1093/nar/gky301

Daniele, S. G., Béraud, D., Davenport, C., Cheng, K., Yin, H., & Maguire-Zeiss, K. A. (2015). Activation of MyD88-dependent TLR1/2 signaling by misfolded α-synuclein, a protein linked to neurodegenerative disorders. *Science Signaling*, *8*(376). https://doi.org/10.1126/scisignal.2005965

Dehay, B., Bourdenx, M., Gorry, P., Przedborski, S., Vila, M., Hunot, S., Singleton, A., Olanow, C. W., Merchant, K. M., Bezard, E., Petsko, G. A., & Meissner, W. G. (2015). Targeting α-synuclein for treatment of Parkinson's disease: Mechanistic and therapeutic considerations. *The Lancet Neurology*, *14*(8), 855–866. https://doi.org/10.1016/S1474-4422(15)00006-X

Donat, C. K., Scott, G., Gentleman, S. M., & Sastre, M. (2017). Microglial Activation in Traumatic Brain Injury. *Frontiers in Aging Neuroscience*, *9*, 208. https://doi.org/10.3389/fnagi.2017.00208

Doorn, K. J., Moors, T., Drukarch, B., van de Berg, W. D., Lucassen, P. J., & van Dam, A.-M. (2014). Microglial phenotypes and toll-like receptor 2 in the substantia nigra and hippocampus of incidental Lewy body disease cases and Parkinson's disease patients. *Acta Neuropathologica Communications*, *2*(1), 90. https://doi.org/10.1186/s40478-014-0090-1

Döring, C., Regen, T., Gertig, U., van Rossum, D., Winkler, A., Saiepour, N., Brück, W., Hanisch, U.-K., & Janova, H. (2017). A presumed antagonistic LPS identifies distinct functional organization of TLR4 in mouse microglia: DöRING et al. *Glia*, *65*(7), 1176–1185. https://doi.org/10.1002/glia.23151

dos-Santos-Pereira, M., Acuña, L., Hamadat, S., Rocca, J., González-Lizárraga, F., Chehín, R., Sepulveda-Diaz, J., Del-Bel, E., Raisman-Vozari, R., & Michel, P. P. (2018). Microglial glutamate release evoked by α-synuclein aggregates is prevented by dopamine. *Glia*, *66*(11), 2353–2365. https://doi.org/10.1002/glia.23472

Drier, Y., Sheffer, M., & Domany, E. (2013). Pathway-based personalized analysis of cancer. *Proceedings of the National Academy of Sciences*, *110*(16), 6388–6393. https://doi.org/10.1073/pnas.1219651110

Dunn, W. B., Broadhurst, D., Begley, P., Zelena, E., Francis-McIntyre, S., Anderson, N., Brown, M., Knowles, J. D., Halsall, A., Haselden, J. N., Nicholls, A. W., Wilson, I. D., Kell, D. B., Goodacre, R., & The Human Serum Metabolome (HUSERMET) Consortium. (2011). Procedures for large-scale metabolic profiling of serum and plasma using gas chromatography and liquid

chromatography coupled to mass spectrometry. *Nature Protocols*, *6*(7), 1060–1083. https://doi.org/10.1038/nprot.2011.335

Dunn, W. B., Wilson, I. D., Nicholls, A. W., & Broadhurst, D. (2012). The importance of experimental design and QC samples in large-scale and MS-driven untargeted metabolomic studies of humans. *Bioanalysis*, *4*(18), 2249–2264. https://doi.org/10.4155/bio.12.204

Fellner, L., Irschick, R., Schanda, K., Reindl, M., Klimaschewski, L., Poewe, W., Wenning, G. K., & Stefanova, N. (2013). Toll-like receptor 4 is required for α-synuclein dependent activation of microglia and astroglia. *Glia*, *61*(3), 349–360. https://doi.org/10.1002/glia.22437

Feng, Y., Zheng, C., Zhang, Y., Xing, C., Cai, W., Li, R., Chen, J., & Duan, Y. (2019). Triptolide Inhibits Preformed Fibril-Induced Microglial Activation by Targeting the MicroRNA155-5p/SHIP1 Pathway. *Oxidative Medicine and Cellular Longevity*, *2019*, 1–13. https://doi.org/10.1155/2019/6527638

Galatro, T. F., Holtman, I. R., Lerario, A. M., Vainchtein, I. D., Brouwer, N., Sola, P. R., Veras, M. M., Pereira, T. F., Leite, R. E. P., Möller, T., Wes, P. D., Sogayar, M. C., Laman, J. D., den Dunnen, W., Pasqualucci, C. A., Oba-Shinjo, S. M., Boddeke, E. W. G. M., Marie, S. K. N., & Eggen, B. J. L. (2017). Transcriptomic analysis of purified human cortical microglia reveals age-associated changes. *Nature Neuroscience*, *20*(8), 1162–1171. https://doi.org/10.1038/nn.4597

Garali, I., Adanyeguh, I. M., Ichou, F., Perlbarg, V., Seyer, A., Colsch, B., Moszer, I., Guillemot, V., Durr, A., Mochel, F., & Tenenhaus, A. (2018). A strategy for multimodal data integration: Application to biomarkers identification in spinocerebellar ataxia. *Briefings in Bioinformatics*, *19*(6), 1356–1369. https://doi.org/10.1093/bib/bbx060

Giacomoni, F., Le Corguille, G., Monsoor, M., Landi, M., Pericard, P., Petera, M., Duperier, C., Tremblay-Franco, M., Martin, J.-F., Jacob, D., Goulitquer, S., Thevenot, E. A., & Caron, C. (2015). Workflow4Metabolomics: A collaborative research infrastructure for computational metabolomics. *Bioinformatics*, *31*(9), 1493–1495. https://doi.org/10.1093/bioinformatics/btu813

Ginhoux, F., Greter, M., Leboeuf, M., Nandi, S., See, P., Gokhan, S., Mehler, M. F., Conway, S. J., Ng, L. G., Stanley, E. R., Samokhvalov, I. M., & Merad, M. (2010). Fate Mapping Analysis Reveals That Adult Microglia Derive from Primitive Macrophages. *Science*, *330*(6005), 841–845. https://doi.org/10.1126/science.1194637

Gribaudo, S., Tixador, P., Bousset, L., Fenyi, A., Lino, P., Melki, R., Peyrin, J.M., Perrier A.L. (2019) Propagation of α-Synuclein strains within human reconstructed neuronal network. *Stem Cell Reports*, 12(2):230-244. doi: 10.1016/j.stemcr.2018.12.007.

Guerrero-Ferreira, R., Taylor, N.M., Arteni, A.A., Kumari, P., Mona, D., Ringler, P., Britschgi, M., Lauer, M.E., Makky, A., Verasdonck, J., Riek, R., Melki, R., Meier, B.H., Böckmann, A., Bousset, L., Stahlberg, H. (2019) Two new polymorphic structures of human full-length alpha-synuclein fibrils solved by cryo-electron microscopy. *Elife*, 8:e48907. doi: 10.7554/eLife.48907.

Guo, J.-J., Yue, F., Song, D.-Y., Bousset, L., Liang, X., Tang, J., Yuan, L., Li, W., Melki, R., Tang, Y., Chan, P., Guo, C., & Li, J.-Y. (2021). Intranasal administration of α-synuclein preformed fibrils triggers microglial iron deposition in the substantia nigra of Macaca fascicularis. *Cell Death & Disease*, *12*(1), 81. https://doi.org/10.1038/s41419-020-03369-x

Gustot, A., Gallea, J. I., Sarroukh, R., Celej, M. S., Ruysschaert, J.-M., & Raussens, V. (2015). Amyloid fibrils are the molecular trigger of inflammation in Parkinson's disease. *Biochemical Journal*, *471*(3), 323–333. https://doi.org/10.1042/BJ20150617

Heneka, M. T., Carson, M. J., Khoury, J. E., Landreth, G. E., Brosseron, F., Feinstein, D. L., Jacobs, A. H., Wyss-Coray, T., Vitorica, J., Ransohoff, R. M., Herrup, K., Frautschy, S. A., Finsen, B., Brown, G. C., Verkhratsky, A., Yamanaka, K., Koistinaho, J., Latz, E., Halle, A., … Kummer, M. P. (2015). Neuroinflammation in Alzheimer's disease. *The Lancet Neurology*, *14*(4), 388–405. https://doi.org/10.1016/S1474-4422(15)70016-5

Hirsch, E. C., & Hunot, S. (2009). Neuroinflammation in Parkinson's disease: A target for neuroprotection? *The Lancet Neurology*, *8*(4), 382–397. https://doi.org/10.1016/S1474-4422(09)70062-6

Hunot, S., Boissière, F., Faucheux, B., Brugg, B., Mouatt-Prigent, A., Agid, Y., & Hirsch, E. C. (1996). Nitric oxide synthase and neuronal vulnerability in parkinson's disease. *Neuroscience*, *72*(2), 355–363. https://doi.org/10.1016/0306-4522(95)00578-1

Kanehisa, M., Goto, S., Sato, Y., Kawashima, M., Furumichi, M., & Tanabe, M. (2014). Data, information, knowledge and principle: Back to metabolism in KEGG. *Nucleic Acids Research*, *42*(D1), D199–D205. https://doi.org/10.1093/nar/gkt1076

Kapralov, A. A., Yang, Q., Dar, H. H., Tyurina, Y. Y., Anthonymuthu, T. S., Kim, R., St. Croix, C. M., Mikulska-Ruminska, K., Liu, B., Shrivastava, I. H., Tyurin, V. A., Ting, H.-C., Wu, Y. L., Gao, Y., Shurin, G. V., Artyukhova, M. A., Ponomareva, L. A., Timashev, P. S., Domingues, R. M., … Kagan, V. E. (2020). Redox lipid reprogramming commands susceptibility of macrophages and microglia to ferroptotic death. *Nature Chemical Biology*, *16*(3), 278–290. https://doi.org/10.1038/s41589-019-0462-8

Keren-Shaul, H., Spinrad, A., Weiner, A., Matcovitch-Natan, O., Dvir-Szternfeld, R., Ulland, T. K., David, E., Baruch, K., Lara-Astaiso, D., Toth, B., Itzkovitz, S., Colonna, M., Schwartz, M., & Amit, I. (2017). A Unique Microglia Type Associated with Restricting Development of Alzheimer's Disease. *Cell*, *169*(7), 1276-1290.e17. https://doi.org/10.1016/j.cell.2017.05.018

Kim, C. C., Nakamura, M. C., & Hsieh, C. L. (2016). Brain trauma elicits non-canonical macrophage activation states. *Journal of Neuroinflammation*, *13*(1), 117. https://doi.org/10.1186/s12974-016-0581-z

Kim, C., Ho, D.-H., Suk, J.-E., You, S., Michael, S., Kang, J., Joong Lee, S., Masliah, E., Hwang, D., Lee, H.-J., & Lee, S.-J. (2013). Neuron-released oligomeric α-synuclein is an endogenous agonist of TLR2 for paracrine activation of microglia. *Nature Communications*, *4*(1), 1562. https://doi.org/10.1038/ncomms2534

Kuleshov, M. V., Jones, M. R., Rouillard, A. D., Fernandez, N. F., Duan, Q., Wang, Z., Koplev, S., Jenkins, S. L., Jagodnik, K. M., Lachmann, A., McDermott, M. G., Monteiro, C. D., Gundersen, G. W., & Ma'ayan, A. (2016). Enrichr: A comprehensive gene set enrichment analysis web server 2016 update. *Nucleic Acids Research*, *44*(W1), W90–W97. https://doi.org/10.1093/nar/gkw377

Landureau, M., Redeker, V., Bellande, T., Eyquem, S., & Melki, R. (2021). The differential solvent exposure of N-terminal residues provides "fingerprints" of alpha-synuclein fibrillar polymorphs. *Journal of Biological Chemistry*, *296*, 100737. https://doi.org/10.1016/j.jbc.2021.100737

Lavaur, J., Le Nogue, D., Lemaire, M., Pype, J., Farjot, G., Hirsch, E. C., & Michel, P. P. (2017). The noble gas xenon provides protection and trophic stimulation to midbrain dopamine neurons. *Journal of Neurochemistry*, *142*(1), 14–28. https://doi.org/10.1111/jnc.14041

Lewerenz, J., Hewett, S. J., Huang, Y., Lambros, M., Gout, P. W., Kalivas, P. W., Massie, A., Smolders, I., Methner, A., Pergande, M., Smith, S. B., Ganapathy, V., & Maher, P. (2013). The

Cystine/Glutamate Antiporter System xc-in Health and Disease: From Molecular Mechanisms to Novel Therapeutic Opportunities. *Antioxidants & Redox Signaling*, *18*(5), 522–555. https://doi.org/10.1089/ars.2011.4391

Lim, S., Chun, Y., Lee, J. S., & Lee, S.-J. (2016). Neuroinflammation in Synucleinopathies: Neuroinflammation in Synucleinopathies. *Brain Pathology*, *26*(3), 404–409. https://doi.org/10.1111/bpa.12371

Locati, M., Curtale, G., & Mantovani, A. (2020). Diversity, Mechanisms, and Significance of Macrophage Plasticity. *Annual Review of Pathology: Mechanisms of Disease*, *15*(1), 123–147. https://doi.org/10.1146/annurev-pathmechdis-012418-012718

Love, M. I., Huber, W., & Anders, S. (2014). Moderated estimation of fold change and dispersion for RNA-seq data with DESeq2. *Genome Biology*, *15*(12), 550. https://doi.org/10.1186/s13059-014-0550-8

Lull, M. E., & Block, M. L. (2010). Microglial activation and chronic neurodegeneration. *Neurotherapeutics*, *7*(4), 354–365. https://doi.org/10.1016/j.nurt.2010.05.014

Marino, M. W., Dunn, A., Grail, D., Inglese, M., Noguchi, Y., Richards, E., Jungbluth, A., Wada, H., Moore, M., Williamson, B., Basu, S., & Old, L. J. (1997). Characterization of tumor necrosis factor-deficient mice. *Proceedings of the National Academy of Sciences*, *94*(15), 8093–8098. https://doi.org/10.1073/pnas.94.15.8093

Massie, A., Schallier, A., Kim, S. W., Fernando, R., Kobayashi, S., Beck, H., Bundel, D. D., Vermoesen, K., Bannai, S., Smolders, I., Conrad, M., Plesnila, N., Sato, H., & Michotte, Y. (2011). Dopaminergic neurons of system $x(c)^-$-deficient mice are highly protected against 6-hydroxydopamine-induced toxicity. *The FASEB Journal*, *25*(4), 1359–1369. https://doi.org/10.1096/fj.10-177212

Massie, A., Schallier, A., Mertens, B., Vermoesen, K., Bannai, S., Sato, H., Smolders, I., & Michotte, Y. (2008). Time-dependent changes in striatal xCT protein expression in hemi-Parkinson rats. *NeuroReport*, *19*(16), 1589–1592. https://doi.org/10.1097/WNR.0b013e328312181c

Mattammal, M. B., Strong, R., Lakshmi, V. M., Chung, H. D., & Stephenson, A. H. (2002). Prostaglandin H Synthetase-Mediated Metabolism of Dopamine: Implication for Parkinson's Disease. *Journal of Neurochemistry*, *64*(4), 1645–1654. https://doi.org/10.1046/j.1471-4159.1995.64041645.x

McCarthy, R. C., Sosa, J. C., Gardeck, A. M., Baez, A. S., Lee, C.-H., & Wessling-Resnick, M. (2018). Inflammation-induced iron transport and metabolism by brain microglia. *Journal of Biological Chemistry*, *293*(20), 7853–7863. https://doi.org/10.1074/jbc.RA118.001949

McFarland, K. N., Ceballos, C., Rosario, A., Ladd, T., Moore, B., Golde, G., Wang, X., Allen, M., Ertekin-Taner, N., Funk, C. C., Robinson, M., Baloni, P., Rappaport, N., Chakrabarty, P., & Golde, T. E. (2021). Microglia show differential transcriptomic response to Aβ peptide aggregates ex vivo and in vivo. *Life Science Alliance*, *4*(7), e202101108. https://doi.org/10.26508/lsa.202101108

Mesci, P., Zaïdi, S., Lobsiger, C. S., Millecamps, S., Escartin, C., Seilhean, D., Sato, H., Mallat, M., & Boillée, S. (2015). System xC− is a mediator of microglial function and its deletion slows symptoms in amyotrophic lateral sclerosis mice. *Brain*, *138*(1), 53–68. https://doi.org/10.1093/brain/awu312

Michel, P. P., Hirsch, E. C., & Hunot, S. (2016). Understanding Dopaminergic Cell Death Pathways in Parkinson Disease. *Neuron*, *90*(4), 675–691. https://doi.org/10.1016/j.neuron.2016.03.038

Mizutani, M., Pino, P. A., Saederup, N., Charo, I. F., Ransohoff, R. M., & Cardona, A. E. (2012). The Fractalkine Receptor but Not CCR2 Is Present on Microglia from Embryonic Development

throughout Adulthood. *The Journal of Immunology*, *188*(1), 29–36. https://doi.org/10.4049/jimmunol.1100421

Mogi, M., Harada, M., Riederer, P., Narabayashi, H., Fujita, K., & Nagatsu, T. (1994). Tumor necrosis factor-α (TNF-α) increases both in the brain and in the cerebrospinal fluid from parkinsonian patients. *Neuroscience Letters*, *165*(1–2), 208–210. https://doi.org/10.1016/0304-3940(94)90746-3

Morganti, J. M., Riparip, L.-K., & Rosi, S. (2016). Call Off the Dog(ma): M1/M2 Polarization Is Concurrent following Traumatic Brain Injury. *PLOS ONE*, *11*(1), e0148001. https://doi.org/10.1371/journal.pone.0148001

Ohgidani, M., Kato, T. A., Setoyama, D., Sagata, N., Hashimoto, R., Shigenobu, K., Yoshida, T., Hayakawa, K., Shimokawa, N., Miura, D., Utsumi, H., & Kanba, S. (2015). Direct induction of ramified microglia-like cells from human monocytes: Dynamic microglial dysfunction in Nasu-Hakola disease. *Scientific Reports*, *4*(1), 4957. https://doi.org/10.1038/srep04957

Orihuela, R., McPherson, C. A., & Harry, G. J. (2016). Microglial M1/M2 polarization and metabolic states: Microglia bioenergetics with acute polarization. *British Journal of Pharmacology*, *173*(4), 649–665. https://doi.org/10.1111/bph.13139

Ouchi, Y., Yagi, S., Yokokura, M., & Sakamoto, M. (2009). Neuroinflammation in the living brain of Parkinson's disease. *Parkinsonism & Related Disorders*, *15*, S200–S204. https://doi.org/10.1016/S1353-8020(09)70814-4

Panicker, N., Sarkar, S., Harischandra, D. S., Neal, M., Kam, T.-I., Jin, H., Saminathan, H., Langley, M., Charli, A., Samidurai, M., Rokad, D., Ghaisas, S., Pletnikova, O., Dawson, V. L., Dawson, T. M., Anantharam, V., Kanthasamy, A. G., & Kanthasamy, A. (2019). Fyn kinase regulates misfolded α-synuclein uptake and NLRP3 inflammasome activation in microglia. *Journal of Experimental Medicine*, *216*(6), 1411–1430. https://doi.org/10.1084/jem.20182191

Peelaerts, W., Bousset, L., Van der Perren, A., Moskalyuk, A., Pulizzi, R., Giugliano, M., Van den Haute, C., Melki, R., & Baekelandt, V. (2015). α-Synuclein strains cause distinct synucleinopathies after local and systemic administration. *Nature*, *522*(7556), 340–344. https://doi.org/10.1038/nature14547

Pereira, M., Chen, T.-D., Buang, N., Olona, A., Ko, J.-H., Prendecki, M., Costa, A. S. H., Nikitopoulou, E., Tronci, L., Pusey, C. D., Cook, H. T., McAdoo, S. P., Frezza, C., & Behmoaras, J. (2019). Acute Iron Deprivation Reprograms Human Macrophage Metabolism and Reduces Inflammation In Vivo. *Cell Reports*, *28*(2), 498-511.e5. https://doi.org/10.1016/j.celrep.2019.06.039

Perry, V. H., Nicoll, J. A. R., & Holmes, C. (2010). Microglia in neurodegenerative disease. *Nature Reviews Neurology*, *6*(4), 193–201. https://doi.org/10.1038/nrneurol.2010.17

Popov, A., Abdullah, Z., Wickenhauser, C., Saric, T., Driesen, J., Hanisch, F.-G., Domann, E., Raven, E. L., Dehus, O., Hermann, C., Eggle, D., Debey, S., Chakraborty, T., Krönke, M., Utermöhlen, O., & Schultze, J. L. (2006). Indoleamine 2,3-dioxygenase–expressing dendritic cells form suppurative granulomas following Listeria monocytogenes infection. *Journal of Clinical Investigation*, *116*(12), 3160–3170. https://doi.org/10.1172/JCI28996

Pozzi, D., Ban, J., Iseppon, F., Torre, V. (2017) An improved method for growing neurons: Comparison with standard protocols. *J Neurosci Methods*, 15:280:1-10. doi: 10.1016/j.jneumeth.2017.01.013.

Prinz, M., Jung, S., & Priller, J. (2019). Microglia Biology: One Century of Evolving Concepts. *Cell*, *179*(2), 292–311. https://doi.org/10.1016/j.cell.2019.08.053

Qin, S. (2006). System Xc- and Apolipoprotein E Expressed by Microglia Have Opposite Effects on the Neurotoxicity of Amyloid-beta Peptide 1-40. *Journal of Neuroscience*, *26*(12), 3345–3356. https://doi.org/10.1523/JNEUROSCI.5186-05.2006

Ransohoff, R. M., & Perry, V. H. (2009). Microglial Physiology: Unique Stimuli, Specialized Responses. *Annual Review of Immunology*, *27*(1), 119–145. https://doi.org/10.1146/annurev.immunol.021908.132528

Reiling, N., Hölscher, C., Fehrenbach, A., Kröger, S., Kirschning, C. J., Goyert, S., & Ehlers, S. (2002). Cutting Edge: Toll-Like Receptor (TLR)2- and TLR4-Mediated Pathogen Recognition in Resistance to Airborne Infection with *Mycobacterium tuberculosis*. *The Journal of Immunology*, *169*(7), 3480–3484. https://doi.org/10.4049/jimmunol.169.7.3480

Rey, N.L., Bousset, L., George, S., Madaj, Z., Meyerdirk, L., Schulz, E., Steiner, J.A., Melki, R., Brundin, P. (2019) α-Synuclein conformational strains spread, seed and target neuronal cells differentially after injection into the olfactory bulb. *Acta Neuropathol Commun*, 7(1):221. doi: 10.1186/s40478-019-0859-3.

Rodríguez-Prados, J.-C., Través, P. G., Cuenca, J., Rico, D., Aragonés, J., Martín-Sanz, P., Cascante, M., & Boscá, L. (2010). Substrate Fate in Activated Macrophages: A Comparison between Innate, Classic, and Alternative Activation. *The Journal of Immunology*, *185*(1), 605–614. https://doi.org/10.4049/jimmunol.0901698

Rook, G. A. W., Steele, J., Umar, S., & Dockrell, H. M. (1985). A simple method for the solubilisation of reduced NBT, and its use as a colorimetric assay for activation of human macrophages by γ-interferon. *Journal of Immunological Methods*, *82*(1), 161–167. https://doi.org/10.1016/0022-1759(85)90235-2

Saeed, A. I., Sharov, V., White, J., Li, J., Liang, W., Bhagabati, N., Braisted, J., Klapa, M., Currier, T., Thiagarajan, M., Sturn, A., Snuffin, M., Rezantsev, A., Popov, D., Ryltsov, A., Kostukovich, E., Borisovsky, I., Liu, Z., Vinsavich, A., … Quackenbush, J. (2003). TM4: A Free, Open-Source System for Microarray Data Management and Analysis. *BioTechniques*, *34*(2), 374–378. https://doi.org/10.2144/03342mt01

Scheiblich, H., Bousset, L., Schwartz, S., Griep, A., Latz, E., Melki, R., & Heneka, M. T. (2021a). Microglial NLRP3 Inflammasome Activation upon TLR2 and TLR5 Ligation by Distinct α-Synuclein Assemblies. *J Immunol*, *207*(8), 2143–2154. https://doi.org/10.4049/jimmunol.2100035

Scheiblich, H., Dansokho, C., Mercan, D., Schmidt, S.V., Bousset, L., Wischhof, L., Eikens, F., Odainic, A., Spitzer, J., Griep, A., Schwartz, S., Bano, D., Latz, E., Melki, R., Heneka, M.T. (2021b) Microglia jointly degrade fibrillar alpha-synuclein cargo by distribution through tunneling nanotubes. *Cell*, 184(20):5089-5106.e21. doi: 10.1016/j.cell.2021.09.007.

Sepulveda-Diaz, J. E., Ouidja, M. O., Socias, S. B., Hamadat, S., Guerreiro, S., Raisman-Vozari, R., & Michel, P. P. (2016). A simplified approach for efficient isolation of functional microglial cells: Application for modeling neuroinflammatory responses *in vitro*: Simplified Approach for Microglia Isolation. *Glia*, *64*(11), 1912–1924. https://doi.org/10.1002/glia.23032

Shahnawaz, M., Mukherjee, A., Pritzkow, S., Mendez, N., Rabadia, P., Liu, X., Hu, B., Schmeichel, A., Singer, W., Wu, G., Tsai, A.-L., Shirani, H., Nilsson, K. P. R., Low, P. A., & Soto, C. (2020). Discriminating α-synuclein strains in Parkinson's disease and multiple system atrophy. *Nature*, *578*(7794), 273–277. https://doi.org/10.1038/s41586-020-1984-7

Shay, J. E. S., & Celeste Simon, M. (2012). Hypoxia-inducible factors: Crosstalk between inflammation and metabolism. *Seminars in Cell & Developmental Biology*, *23*(4), 389–394. https://doi.org/10.1016/j.semcdb.2012.04.004

Shrivastava, A.N., Bousset, L., Renner, M., Redeker, V., Savistchenko, J., Triller, A., Melki, R. (2020) Differential membrane binding and seeding of distinct α-Synuclein fibrillar polymorphs. *Biophys J,* 118(6):1301-1320. doi: 10.1016/j.bpj.2020.01.022.

Smith, C. A., Want, E. J., O'Maille, G., Abagyan, R., & Siuzdak, G. (2006). XCMS: Processing Mass Spectrometry Data for Metabolite Profiling Using Nonlinear Peak Alignment, Matching, and Identification. *Analytical Chemistry*, *78*(3), 779–787. https://doi.org/10.1021/ac051437y

Song, S.-Y., Kim, I.-S., Koppula, S., Park, J.-Y., Kim, B.-W., Yoon, S.-H., & Choi, D.-K. (2020). 2-Hydroxy-4-Methylbenzoic Anhydride Inhibits Neuroinflammation in Cellular and Experimental Animal Models of Parkinson's Disease. *International Journal of Molecular Sciences*, *21*(21), 8195. https://doi.org/10.3390/ijms21218195

Szulzewsky, F., Pelz, A., Feng, X., Synowitz, M., Markovic, D., Langmann, T., Holtman, I. R., Wang, X., Eggen, B. J. L., Boddeke, H. W. G. M., Hambardzumyan, D., Wolf, S. A., & Kettenmann, H. (2015). Glioma-Associated Microglia/Macrophages Display an Expression Profile Different from M1 and M2 Polarization and Highly Express Gpnmb and Spp1. *PLOS ONE*, *10*(2), e0116644. https://doi.org/10.1371/journal.pone.0116644

Tansey, M. G., & Goldberg, M. S. (2010). Neuroinflammation in Parkinson's disease: Its role in neuronal death and implications for therapeutic intervention. *Neurobiology of Disease*, *37*(3), 510–518. https://doi.org/10.1016/j.nbd.2009.11.004

Tautenhahn, R., Patti, G. J., Rinehart, D., & Siuzdak, G. (2012). XCMS Online: A Web-Based Platform to Process Untargeted Metabolomic Data. *Analytical Chemistry*, *84*(11), 5035–5039. https://doi.org/10.1021/ac300698c

Teismann, P., Tieu, K., Choi, D.-K., Wu, D.-C., Naini, A., Hunot, S., Vila, M., Jackson-Lewis, V., & Przedborski, S. (2003). Cyclooxygenase-2 is instrumental in Parkinson's disease neurodegeneration. *Proceedings of the National Academy of Sciences*, *100*(9), 5473–5478. https://doi.org/10.1073/pnas.0837397100

Teismann, P., Tieu, K., Cohen, O., Choi, D.-K., Wu, D. C., Marks, D., Vila, M., Jackson-Lewis, V., & Przedborski, S. (2003). Pathogenic role of glial cells in Parkinson's disease. *Movement Disorders*, *18*(2), 121–129. https://doi.org/10.1002/mds.10332

Tourville, A., Akbar, D., Corti, O., Prehn, J.H.M., Melki, R., Hunot, S., Michel, P.P. (2022) Modelling α-Synuclein Aggregation and Neurodegeneration with Fibril Seeds in Primary Cultures of Mouse Dopaminergic Neurons. *Cells*, 13;11(10):1640. doi: 10.3390/cells11101640.

Tu, D., Gao, Y., Yang, R., Guan, T., Hong, J.-S., & Gao, H.-M. (2019). The pentose phosphate pathway regulates chronic neuroinflammation and dopaminergic neurodegeneration. *Journal of Neuroinflammation*, 16(1), 1–17. https://doi.org/10.1186/s12974-019-1659-1

Van der Perren, A., Gelders, G., Fenyi, A., Bousset, L., Brito, F., Peelaerts, W., Van den Haute, C., Gentleman, S., Melki, R., & Baekelandt, V. (2020). The structural differences between patient-derived α-synuclein strains dictate characteristics of Parkinson's disease, multiple system atrophy and dementia with Lewy bodies. *Acta Neuropathologica*, 139(6), 977–1000. https://doi.org/10.1007/s00401-020-02157-3

Veselkov, K. A., Vingara, L. K., Masson, P., Robinette, S. L., Want, E., Li, J. V., Barton, R. H., Boursier-Neyret, C., Walther, B., Ebbels, T. M., Pelczer, I., Holmes, E., Lindon, J. C., & Nicholson, J. K.

(2011). Optimized Preprocessing of Ultra-Performance Liquid Chromatography/Mass Spectrometry Urinary Metabolic Profiles for Improved Information Recovery. *Analytical Chemistry*, *83*(15), 5864–5872. https://doi.org/10.1021/ac201065j

Wang, J., Wang, F., Mai, D., & Qu, S. (2020). Molecular Mechanisms of Glutamate Toxicity in Parkinson's Disease. *Frontiers in Neuroscience*, 14, 585584. https://doi.org/10.3389/fnins.2020.585584

Want, E. J., Wilson, I. D., Gika, H., Theodoridis, G., Plumb, R. S., Shockcor, J., Holmes, E., & Nicholson, J. K. (2010). Global metabolic profiling procedures for urine using UPLC–MS. *Nature Protocols*, *5*(6), 1005–1018. https://doi.org/10.1038/nprot.2010.50

Warburg O. On respiratory impairment in cancer cells. Science. (1956) 124:269–70. doi: 10.1126/science.124.3215.267

Wu, Y.-R., Feng, I.-H., Lyu, R.-K., Chang, K.-H., Lin, Y.-Y., Chan, H., Hu, F.-J., Lee-Chen, G.-J., & Chen, C.-M. (2007). Tumor necrosis factor-α promoter polymorphism is associated with the risk of Parkinson's disease. *American Journal of Medical Genetics Part B: Neuropsychiatric Genetics*, *144B*(3), 300–304. https://doi.org/10.1002/ajmg.b.30435

Xie, Z., Bailey, A., Kuleshov, M. V., Clarke, D. J. B., Evangelista, J. E., Jenkins, S. L., Lachmann, A., Wojciechowicz, M. L., Kropiwnicki, E., Jagodnik, K. M., Jeon, M., & Ma'ayan, A. (2021). Gene Set Knowledge Discovery with Enrichr. *Current Protocols*, *1*(3). https://doi.org/10.1002/cpz1.90

Xue, J., Schmidt, S. V., Sander, J., Draffehn, A., Krebs, W., Quester, I., De Nardo, D., Gohel, T. D., Emde, M., Schmidleithner, L., Ganesan, H., Nino-Castro, A., Mallmann, M. R., Labzin, L., Theis, H., Kraut, M., Beyer, M., Latz, E., Freeman, T. C., … Schultze, J. L. (2014). Transcriptome-Based Network Analysis Reveals a Spectrum Model of Human Macrophage Activation. *Immunity*, *40*(2), 274–288. https://doi.org/10.1016/j.immuni.2014.01.006

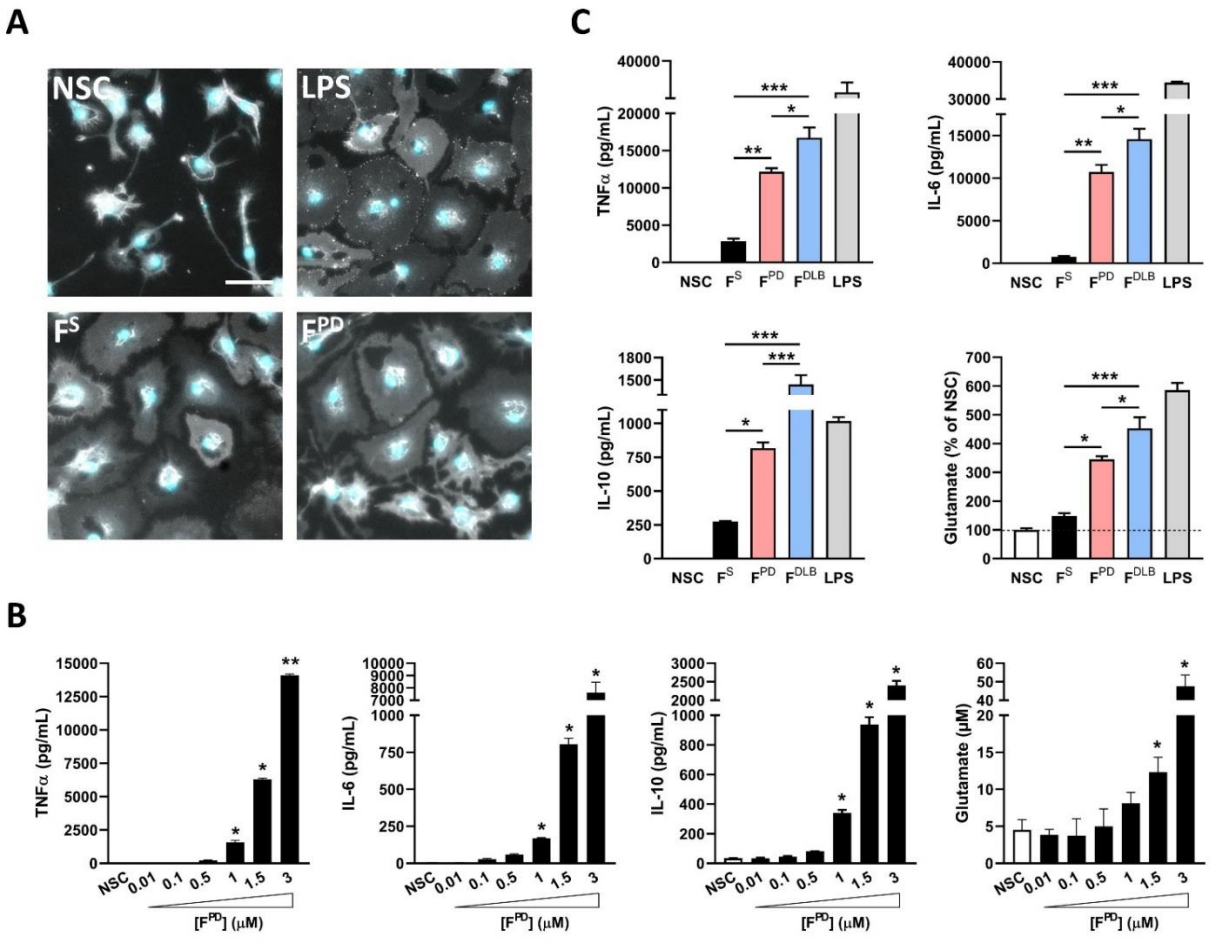

Figure 1. Human αSYN fibrils derived from PD patients by PMCA hold more potent inflammatory properties than *de novo* generated counterparts. (**A**) Representative images of CD11b immunostaining and Hoechst nuclear stain (blue) showing the morphological changes of microglial cells following inflammatory stimulation by the prototypal inflammogen LPS (10ng/ml), *de novo* assembled human αSYN fibrils (3µM; F^S) and fibrils derived from PD patients (3µM; F^{PD}). Note that inflammatory stimulation results in cellular flattering and shortening of cell processes in all three inflammatory conditions. Scale bar: 50µm. (**B**) Dose-response analysis of TNFα, IL6, IL10 and glutamate release by microglial cells exposed or not (NSC) to increasing concentrations (from 0.01 to 3µM) of αSYN fibrils derived from PD patients (F^{PD}). Data are means ± SEM (n = 6). *$p < 0.05$; **$p < 0.01$ vs. NSC (Tukey's test). (**C**) Quantification of TNFα, IL6, IL10 and glutamate release by microglial cells exposed

or not (NSC) to similar concentrations of F^S, F^{PD} or F^{DLB} (3µM). Data are means ± SEM (n = 6). *$p < 0.05$; **$p < 0.01$; ***$p < 0.001$ vs. F^S (Tukey's test).

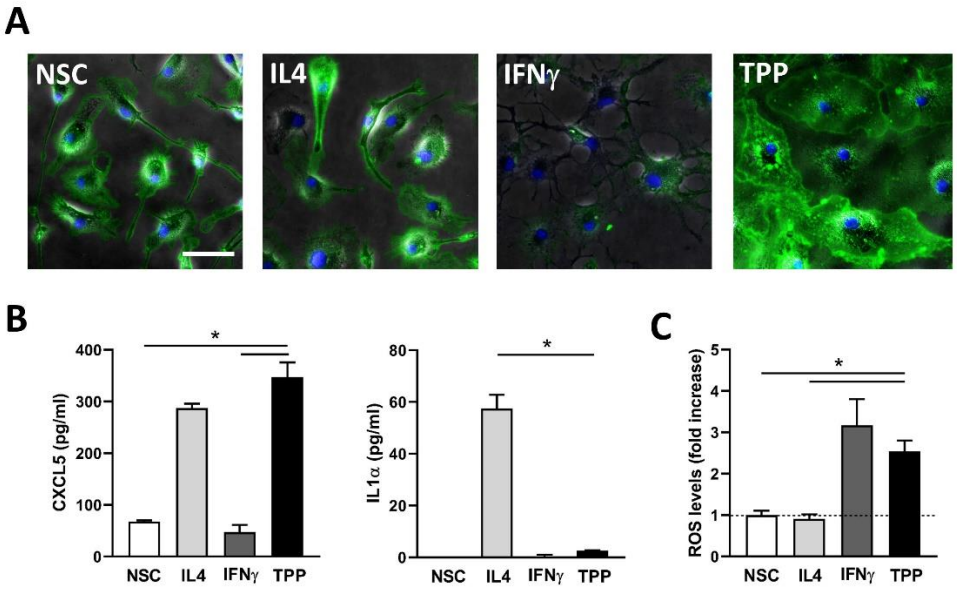

Figure 2. Regulation of human macrophage-associated TPP-specific inflammatory markers in microglial cells. (**A**) Representative images showing CD25 immunostaining with Hoechst nuclear stain (blue) in non-stimulated microglial cells (NSC) and cells exposed to IL4 (10ng/mL), IFNγ (20ng/mL) or a combination of TNFα (800 UI/ml), PGE_2 (1µg/ml) and Pam3C (1µg/ml) (TPP stimulation). Scale bar: 60µm. (**B**) Quantification of CXCL5 and IL1α release by microglial cells exposed or not (NSC) to the indicated treatments. Data are means ± SEM (n = 4). *p < 0.05 vs. TPP (Tukey's test). (**C**) Quantification of ROS production measured with the NBT reaction in microglial cells exposed or not (NSC) to the indicated treatments. Data are means ± SEM (n = 4). *p < 0.05 vs. TPP (Tukey's test).

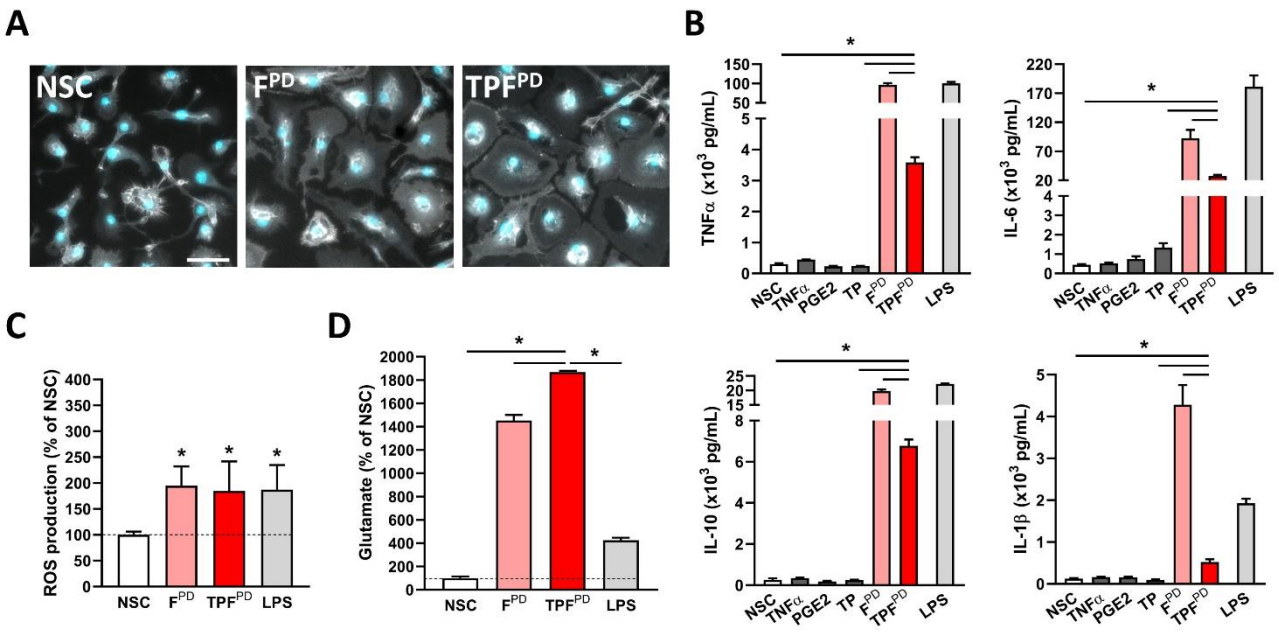

Figure 3. TPF^{PD}-related chronic-type inflammatory stimulation of microglial cells is associated with lower cytokine but increased glutamate release. (**A**) Representative images of CD11b immunostaining and Hoechst nuclear stain (blue) of microglial cells following inflammatory stimulation by PD patients-derived αSYN fibrils (1.5 µM; F^{PD}) or TPF^{PD} as compared to non-stimulated cells (NSC). Note that F^{PD} and TPF^{PD} induces similar morphological changes of microglial cells. Scale bar: 50µm. (**B**) Quantification of TNFα, IL6, IL10 and IL1β release by microglial cells exposed or not (NSC) to TNFα (800 IU/mL), PGE_2 (1 µg/mL), TNFα+PGE_2 (TP), F^{PD} (1.5 µM), TNFα+PGE_2+F^{PD} (TPF^{PD}) or LPS (10 ng/mL). Data are means ± SEM (n = 3-6). *p < 0.05; **p < 0.01; ***p < 0.001 vs. F^{S} (Student's t-test). (**C**) Quantification of ROS production measured by the NBT reaction in microglial cells exposed or not (NSC) to F^{PD} (1.5 µM), TPF^{PD} or LPS (10 ng/mL). Data are expressed as % of NSC control. Bars are means ± SEM (n = 6). *p < 0.05 vs. NSC (Student's t-test). (**D**) Quantification of glutamate release by microglial cells exposed or not (NSC) to F^{PD} (1.5 µM), TPF^{PD} or LPS (10ng/mL). Data are expressed as % of NSC control. Bars are means ± SEM (n = 3-6). *p < 0.05 vs. TPF^{PD} (Tukey's test).

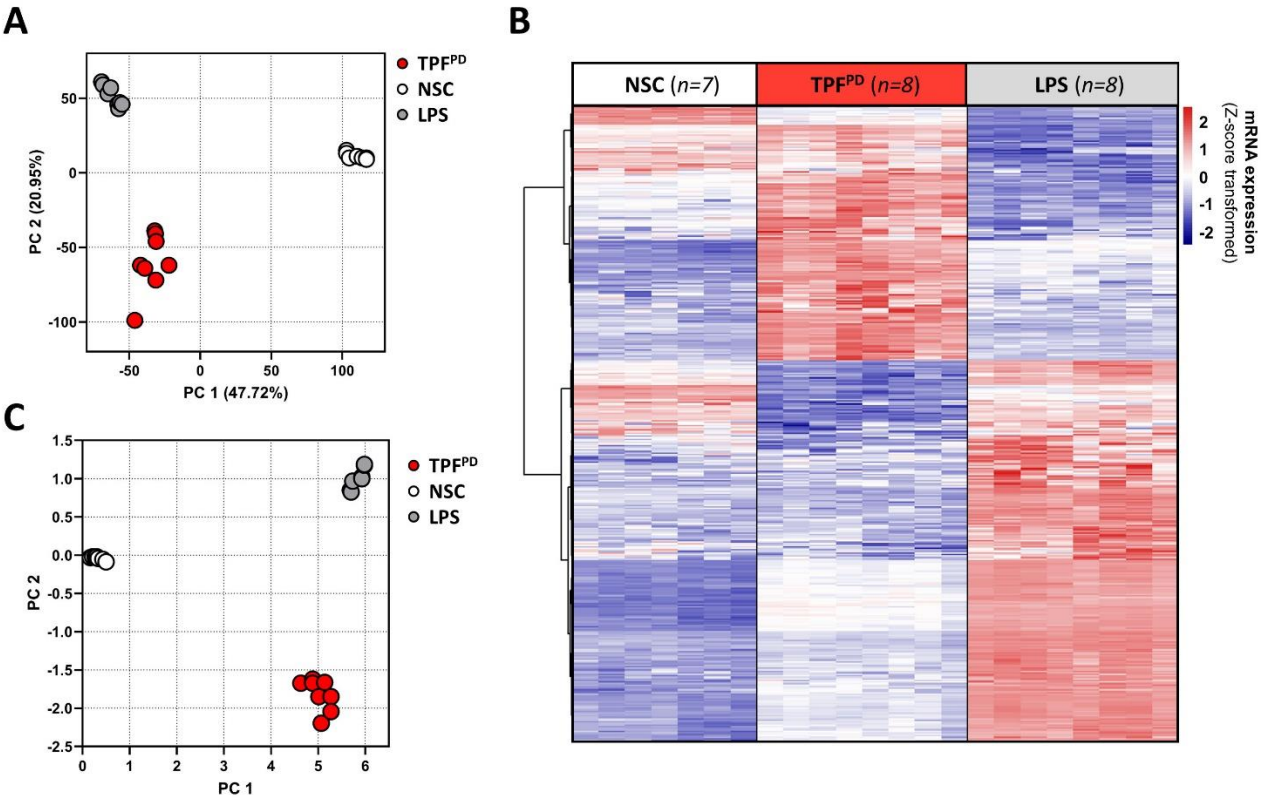
A
TPF^PD
NSC
LPS
PC 2 (20.95%)
PC 1 (47.72%)
B
NSC (n=7)
TPF^PD (n=8)
LPS (n=8)
mRNA expression
(Z-score transformed)
C
PC 2
PC 1

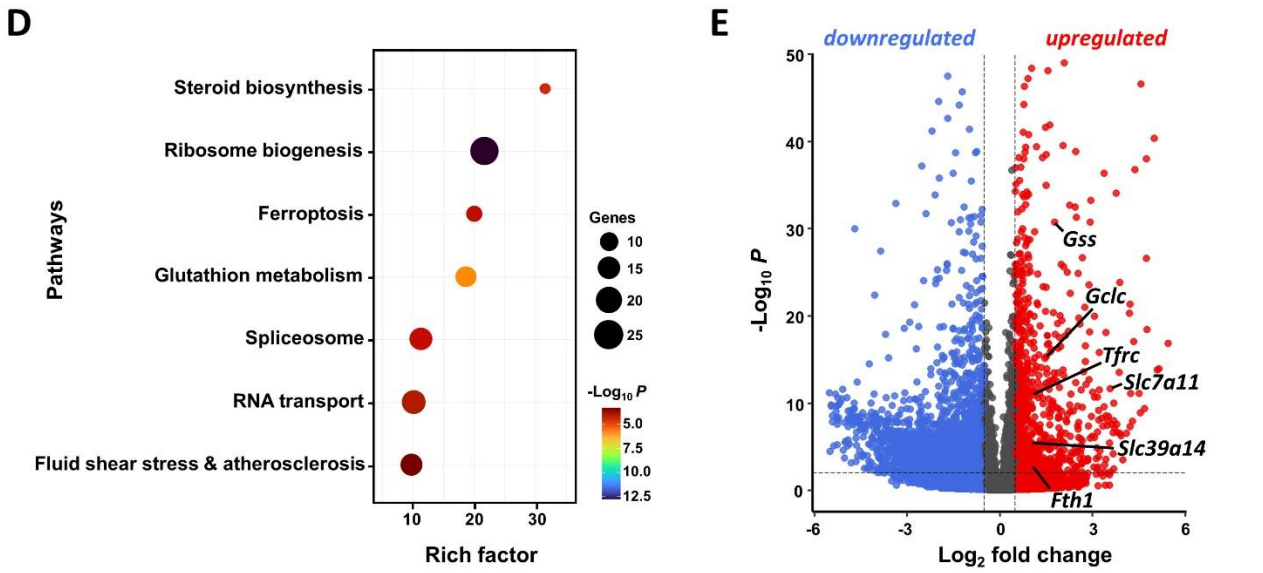
D
Pathways
Steroid biosynthesis
Ribosome biogenesis
Ferroptosis
Glutathion metabolism
Spliceosome
RNA transport
Fluid shear stress & atherosclerosis
Genes
-Log10 P
Rich factor
E
downregulated
upregulated
-Log10 P
Log2 fold change
Gss
Gclc
Tfrc
Slc7a11
Slc39a14
Fth1

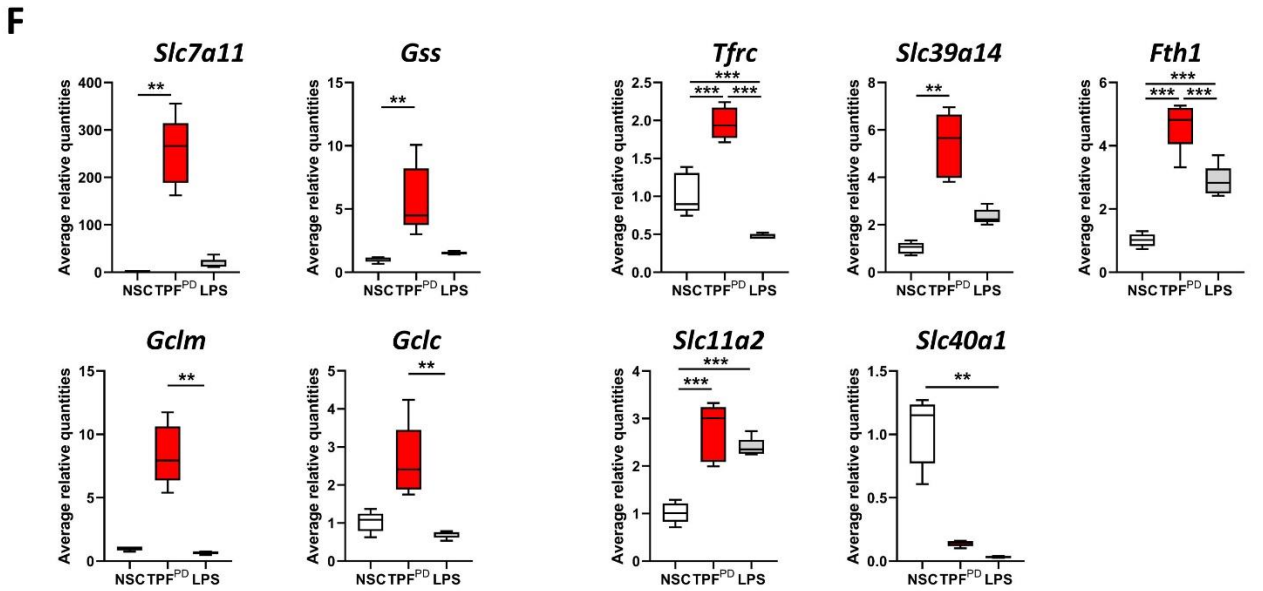
F
Slc7a11
Gss
Tfrc
Slc39a14
Fth1
Gclm
Gclc
Slc11a2
Slc40a1
Average relative quantities
NSC TPF^PD LPS

Figure 4. Specific transcriptional reprogramming of microglial cells upon TPF^{PD} chronic-type inflammatory activation. (**A**) Principal component analysis (PCA) of gene expression data based on the first two PCs shows on one hand clear distinction between non stimulated (NSC) and activated cells (LPS and TPF^{PD}) and, on the other hand, strong differences between M1-type (LPS) and chronic-type (TPF^{PD}) inflammatory activation. (**B**) Hierarchical clustering and heat map of differentially expressed genes (DEGs; n=413) in TPF^{PD}-activated microglia versus non stimulated (NSC) and LPS-treated cells. The scaled expression value (Z-score transformed) is shown in a blue-red color scheme with red indicating higher expression, and blue lower expression. Biological replicates are indicated in brackets. (**C**) PCA analysis of pathway-related data generated by the Pathifier method (Drier et al., 2013) demonstrates clear clustering and separation of stimulated and non-stimulated (NSC) cells and of M1-type (LPS) and chronic-type (TPF^{PD}) inflammatory activation. (**D**) Bubble chart showing the enrichment of the KEGG Pathway in TPF^{PD}-treated microglial cells (adjusted $p < 0.05$). Bubble size indicates the number of genes annotated in the indicated KEGG pathway. Colors represent pathway enrichment (% of overlapping genes) in TPF^{PD}-exposed cells. (**E**) Volcano plot depicting individual DEGs ($|\text{Log}_2 \text{ Fold Change}| > 2$) in TPF^{PD}-treated microglia versus M1-type (LPS) activated cells. Red and blue dots show upregulated and downregulated genes in TPF^{PD}-treated cells, respectively. Individual genes of interest are indicated. (**F**) Relative gene expression analysis (qPCR) of individual gene candidates in non-stimulated- (NSC), LPS-activated and TPF^{PD}-exposed microglial cells. Data are means ± SEM (n=5 biological replicates from independent experiment). $^*p < 0.05$ vs TPF^{PD} (Student's t test).

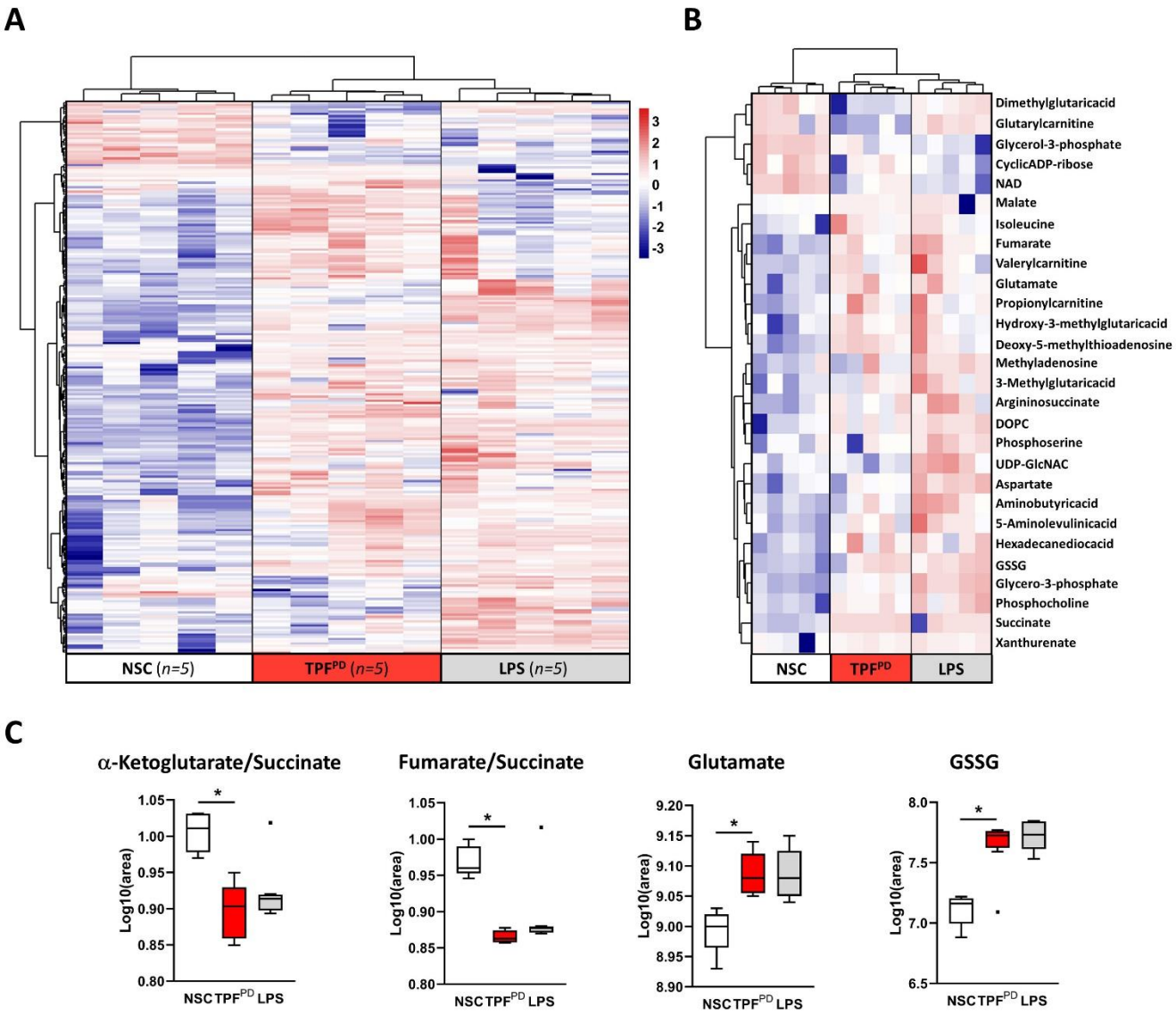

Figure 5. Microglial metabolic reprogramming evoked by TPF^{PD} is closely related to M1-type polarized cells. (**A**) Hierarchical clustering analysis and heatmap visualization of 248 differentially regulated metabolites (28 annotated and 220 unknown/non-annotated metabolites) in stimulated cells (LPS and TPF^{PD}) compared to NSC control. Number of biological replicates are indicated in brackets. Clear changes in the metabolic profile between stimulated and non-stimulated cells can be observed. (**B**) Hierarchical clustering analysis and heatmap visualization of the 28 annotated metabolites extracted from (A). Despite subtle differences, TPF^{PD}- and LPS-associated metabolic signature are closely related. (**C**) Box graphs showing the relative amount of a-ketoglutarate, succinate,

fumarate, glutamate and glutathione disulfide (GSSG) in control (NSC), LPS- and TPF^{PD}-treated microglial cells. A similar decrease in the a-ketoglutarate/succinate and fumarate/succinate ratios was found in LPS- and TPF^{PD}-stimulated cells. Likewise, a similar increase in glutamate and GSSG levels was observed in both stimulatory conditions. *$p < 0.05$ (Kruskall Wallis & Wicoxon test).

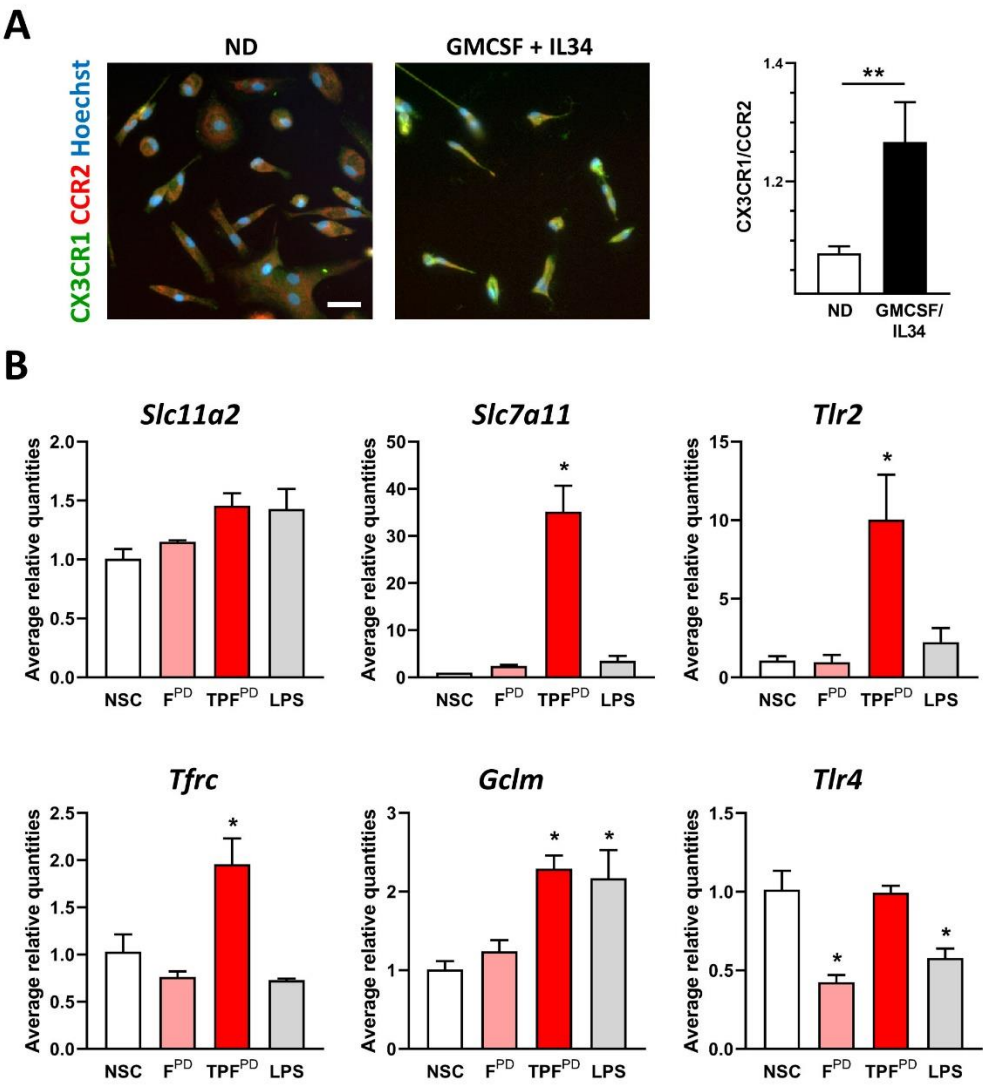

Figure 6. TPF^{PD}-exposed human microglial-like cells display both conserved and distinct gene regulation compared to mouse microglia. (**A**) Representative images showing CCR2 (red) and CX3CR1 (green) double immunostaining with Hoechst nuclear stain (blue) on non-differentiated (ND) and GM-CSF/IL34-differentiated human monocytes (iMG) after 16 days of culture. Right panel shows quantification of the immuno-signal CX3CR1/CRR2 ratio in ND and GM-CSF/IL34-differentiated cells. Data are means ± SEM (n = 4-5). **$p < 0.01$ vs. ND (Student's t-test). Scale bar: 40µm (**B**) Relative expression analysis (qPCR) of individual gene candidates in non-stimulated (NSC), LPS-, F^{PD}- and TPF^{PD}-activated iMGs. Data are means ± SEM (biological replicates n=3). *$p < 0.05$ vs. TPF^{PD} (Student's t test).

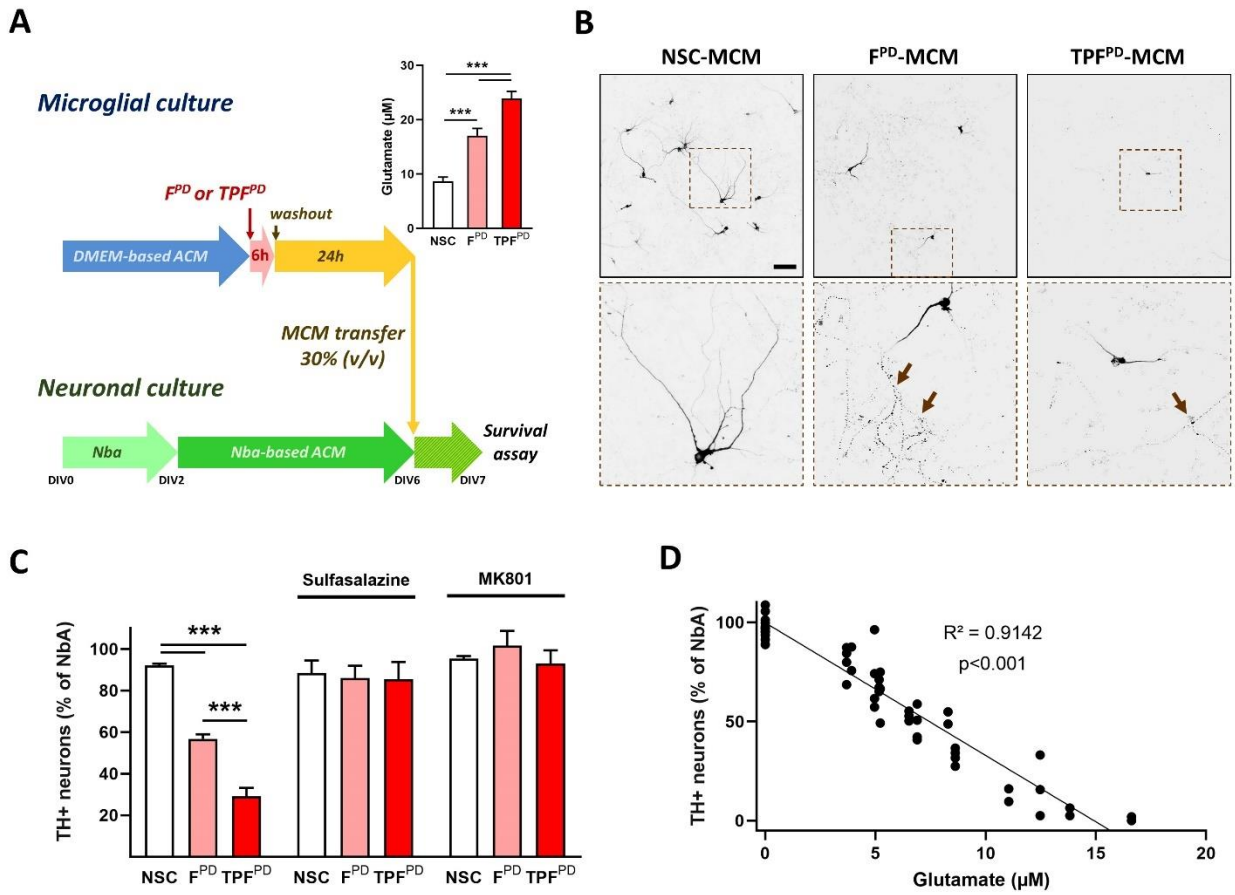

Figure 7. TPF^{PD}-stimulated microglial cells trigger higher excitotoxic cell death than F^{PD}-exposed cells on dopaminergic neurons. (**A**) Schematic representation of the experimental setup used to analyze the neurotoxic potential of chronic-type inflammatory microglial cells. Microglial cell cultures were maintained in DMEM-based astrocyte-conditioned medium (ACM) and exposed or not (NSC) for 6 hours to either F^{PD} or TPF^{PD}. Following inflammatory stimulation, culture medium was fully replaced with fresh DMEM-based ACM (washout step) and microglial cells were let for 24 hours before glutamate assay (upper left graph) and microglial-conditioned media (MCM) transfer to neuronal cultures. Midbrain neuronal cultures were prepared from E13.5 mouse embryos and maintained for 2 days in Neurobasal-A culture medium (Nba). At day *in vitro* 2 (DIV2), culture medium was fully replaced by Nba-based ACM and neurons were let to mature until DIV6. At DIV6, 30% of Nba-based ACM media

was replaced by MCM and TH+ dopaminergic neuron survival was assayed 24 hours later. Data are means ± SEM (biological replicates n=13; 3 independent experiments). ***$p < 0.001$ vs. NSC and F^{PD} (One-way ANOVA followed by Tukey test). (**B**) Low and higher (dashed brown squares) magnification images from DIV7 midbrain cultures exposed for 24 hours to MCM from F^{PD} and TPF^{PD}-stimulated or unstimulated cells (NSC). Brown arrows point to dystrophic cell bodies and processes with varicosities. Scale Bar = 100 µm. (**C**) Survival of TH+ neurons in DIV7 midbrain cultures exposed for 24 hours to MCM from F^{PD} and TPF^{PD}-stimulated or unstimulated cells (NSC). In sister cultures, neurons were exposed to MCM from F^{PD} and TPF^{PD}-stimulated microglial cells treated with the xCT inhibitor Sulfasalazine (250 µM) during the 24hr washout period. In additional sister cultures, neurons exposed to MCM from F^{PD} and TPF^{PD}-stimulated microglial cells were co-treated with the N-Methyl-D-aspartate (NMDA) receptor pore blocker MK-801 (2 µM). Data are means ± SEM (biological replicates n=13; 3 independent experiments). *** $p < 0.001$ vs. NSC or F^{PD} (One-way ANOVA followed by pairwise multiple comparison using the Holm-Sidak method). (**D**) TH+ dopaminergic neuron survival is inversely correlated to the concentration of glutamate within transferred MCM (linear regression analysis).